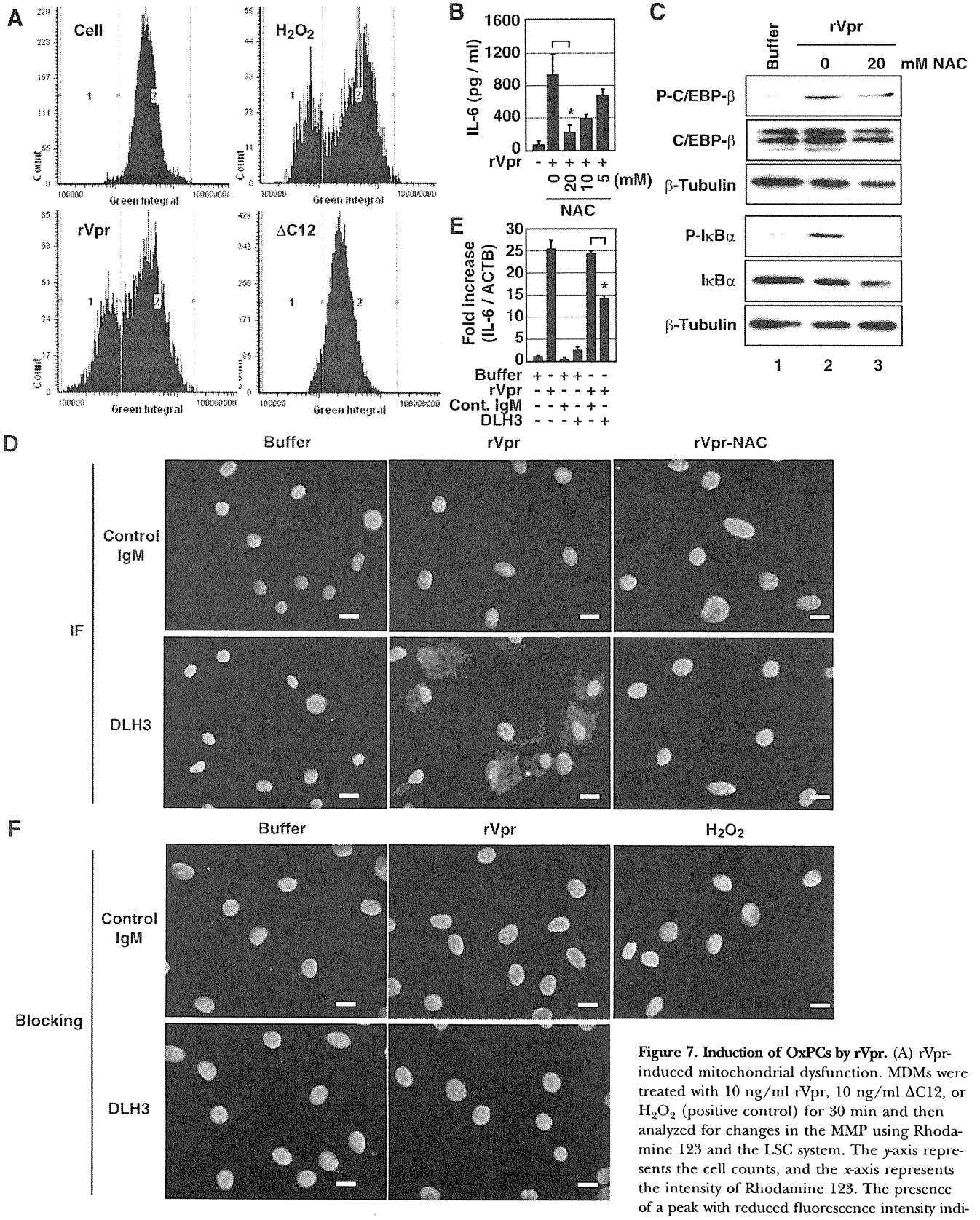

Figure 7. Induction of OxPCs by rVpr. (A) rVpr-induced mitochondrial dysfunction. MDMs were treated with 10 ng/ml rVpr, 10 ng/ml ΔC12, or H_2O_2 (positive control) for 30 min and then analyzed for changes in the MMP using Rhodamine 123 and the LSC system. The *y*-axis represents the cell counts, and the *x*-axis represents the intensity of Rhodamine 123. The presence of a peak with reduced fluorescence intensity indicates a decrease in the MMP [17]. (B) NAC inhibited rVpr-induced IL-6 production. MDMs were treated with NAC at 5, 10, or 20 mM in the presence of 10 ng/ml rVpr for 2 days. (C) The rVpr-induced phosphorylation of C/EBP-β and IκB-α was inhibited by NAC. MDMs were treated with 10 ng/ml rVpr in the presence (lane 3) or

(*continued on next page*)

As Vpr was reported to activate the NF-κB and MAPK pathways [36], we next examined the functional linkage of IκB-α phosphorylation with rVpr-induced IL-6 production. First, we observed that SS, a known inhibitor of IKK [37], blocked rVpr-induced IL-6 production from PBMCs (Fig. 2B) and MDMs (Fig. 2C). Consistent with this, we found that IκB-α was phosphorylated by rVpr (Fig. 2D, lane 3). To examine further the importance of IκB-α phosphorylation in *IL-6* transcription, we prepared a Vpr mutant lacking the ΔC12 (Fig. 2E). Previously, we found that the C-terminal region of Vpr was important for its function, and among several mutants lacking various lengths of the C-terminal region, ΔC12 was almost totally defective in terms of its biological activity compared with wild-type Vpr [38]. Compared with rVpr, ΔC12 showed significantly less ability to induce IL-6 production ($P<0.05$: Fig. 2, F and G). This mutant, however, induced the phosphorylation of IκB-α to a level comparable with that of rVpr (Fig. 2D, lane 4). These data indicate that rVpr-induced IL-6 production depends on the NF-κB pathway but that additional cellular factors are also required.

C/EBP-β is a pivotal factor in rVpr-induced IL-6 production

We next studied the involvement of AP-1 and C/EBP-β in rVpr-induced IL-6 production. WB analysis revealed that AP-1 was activated by rVpr and ΔC12 (**Fig. 3A**, middle column, lane 3), whereas C/EBP-β was activated selectively by rVpr (Fig. 3A, top column, lane 2). Additionally, SB202190, a specific inhibitor of p38, attenuated rVpr-induced IL-6 production ($P<0.05$; Fig. 3B, indicated by *) with concomitant inhibition of rVpr-induced C/EBP-β phosphorylation (Fig. 3C, lane 3). Moreover, SB202190 blocked viral production in U1 cells cocultured with PBMCs and rVpr ($P<0.05$; Fig. 3D). These observations indicate that C/EBP-β is a pivotal factor in rVpr-induced IL-6 production and viral production. To demonstrate this, we tested the effects of C/EBP-β siRNA on rVpr activity. Consistent with the data obtained using SB202190 (Fig. 3B), the knockdown of endogenous C/EBP-β expression abrogated rVpr-induced IL-6 production ($P<0.05$; Fig. 3, E and F).

To highlight further the importance of C/EBP-β in rVpr-induced IL-6 production, we conducted complementation experiments. As shown in **Figure 4A**, U1 (lane 3), its parental cell line U937 (lane 2), and THP-1 (lane 5), another human monocytic leukemia cell line, expressed low levels of endogenous C/EBP-β compared with MDMs (lanes 1 and 4). These three cell lines did not respond to rVpr by producing IL-6 (data not shown); however, the forced expression of exogenous *C/EBP-β* cDNA in leukemic cells (Fig. 4A, lane 7) made the cells competent for rVpr ($P<0.05$; Fig. 4B)- and LPS-induced IL-6 production ($P<0.05$; Fig. 4C). These results indicate that C/EBP-β is a pivotal factor in rVpr activity. Intriguingly, ΔC12 induced less IL-6, even under these conditions ($P<0.05$; Fig. 4B).

rVpr-induced IL-6 production depends on MyD88 and TLR4

To explore the involvement of the TLR signaling cascade in the modulation of NF-κB and MAPK by rVpr, we first examined the effects of the down-regulation of endogenous MyD88 on IL-6 production. The introduction of MyD88 siRNA into MDMs efficiently repressed endogenous MyD88 expression and responsiveness to LPS (**Fig. 5A** and Supplemental Fig. 6). Next, we examined the responsiveness to rVpr and found that rVpr-induced IL-6 production was attenuated significantly by the siRNA ($P<0.05$; Fig. 5B). We further characterized the phosphorylation status of several cellular proteins after the down-regulation of endogenous MyD88. Introduction of the siRNA reduced the rVpr-induced phosphorylation of IκB-α, C/EBP-β, and c-Jun significantly (Fig. 5C, compare lanes 3 and 6). Interestingly, the total amount of IκB-α was increased by rVpr (Fig. 5C, second column from the top, lane 6) but not by LPS. We obtained the same results in three independent experiments, suggesting that Vpr affects the processing of IκB-α, as postulated by Ayyavoo et al. [15].

Next, we examined the involvement of TLR molecules in this process. Among the TLR members tested, TLR2 and TLR4 were of primary interest, as these molecules were reported to interact with viral proteins [22, 23]. As an initial trial, we tested the effects of neutralizing antibodies against TLR2 and TLR4 and found that an anti-TLR4 antibody attenuated IL-6 production by rVpr ($P<0.05$; **Table 1**). We next analyzed the effects of TLR4 siRNA on rVpr-induced IL-6 production. The down-regulation of endogenous TLR4 was confirmed by RT-PCR (**Fig. 6A**), immunohistochemical analysis ($P<0.05$; Fig. 6, B and C), and LPS responsiveness testing ($P<0.05$; Fig. 6D). Two independent experiments were done using MDMs prepared from different healthy donors; both trials revealed that TLR4 siRNA attenuated rVpr-induced IL-6 production significantly ($P<0.05$; Fig. 6E).

rVpr-induced OxPC formation stimulates IL-6 production

Based on our results showing that rVpr-induced IL-6 production depended on TLR4/MyD88, we expected that rVpr would bind TLR4 directly. To demonstrate this, we examined the molecular interaction between rTLR4 proteins and rVpr using the Biacore system but obtained no positive results (data not shown). As another possibility, we hypothesized that TLR4/

absence (lanes 1 and 2) of 20 mM NAC. For the analysis of IκB-α, cells were treated with 150 μM ALLN. (D) Induction of OxPCs by rVpr. MDMs were treated with 10 ng/ml rVpr in the presence or absence of 20 mM NAC. Thereafter, the cells were fixed and stained using DLH3. Red, OxPCs; blue, nucleus; original scale bars, 10 μm. IF, immunofluorescence. (E) rVpr-induced IL-6 production was blocked by inhibiting the induction of OxPCs. MDMs were treated with 10 ng/ml rVpr in the presence or absence of 20 nM DLH3. mRNA samples were then collected, and the level of IL-6 expression was analyzed by RT-qPCR. ACTB was included as a loading control. (F) The rVpr-induced phosphorylation of C/EBP-β was blocked by inhibiting the induction of OxPCs. MDMs were treated with rVpr in the presence or absence of 20 nM DLH3. Thereafter, the cells were fixed and stained using α-phosphorylated C/EBP-β. Red, phosphorylated C/EBP-β; blue, nuclear DNA; original scale bars, 10 μm. The data were obtained from three independent experiments. The values are expressed as the mean ± SD. *, $P < 0.05$.

MyD88-dependent pathways were modulated by rVpr-induced oxidative stress and OxPC.

To investigate the involvement of OxPC in triggering rVpr-induced cellular responses, we first sought to determine whether IL-6 production was coupled with rVpr-induced oxidative stress by testing for changes in the MMP, an indicator of oxidative stress [17]. As observed in MDMs treated with H_2O_2 as a positive control (**Fig. 7A**, upper right panel), we found that rVpr generated a peak that was shifted to the left on the *x*-axis, indicating a decrease in the MMP (Fig. 7A, lower left panel; peak 1). In contrast, ΔC12 did not induce a shift (Fig. 7A, lower right panel; only peak 2 is observed). To show the importance of ROS in rVpr-induced IL-6 production, we next examined the effects of NAC on rVpr-induced cellular responses (Fig. 7B). As shown in Figure 7C, NAC decreased the rVpr-induced phosphorylation of C/EBP-β and IκB-α (Fig. 7C, compare lanes 2 and 3). We then examined the formation of OxPC following the addition of rVpr to MDMs. Interestingly, the mAb DLH3 [33, 34] detected OxPC, formed after treatment of rVpr (Fig. 7D, lower middle panel). The rVpr-induced formation of OxPC was blocked by the addition of NAC (Fig. 7D, lower right panel). Moreover, pretreatment of the MDMs with DLH3 attenuated rVpr-induced IL-6 production ($P<0.05$; Fig. 7E) and the phosphorylation of C/EBP-β (Fig. 7F, compare the upper middle and lower middle panels). These data suggest that OxPC, generated by rVpr-induced oxidative stress, modulate TLR4/MyD88 signaling and induce IL-6 production via the phosphorylation of C/EBP-β.

DISCUSSION

In this study, we found that rVpr activated the TLR4/MyD88-dependent cellular cascade in human MDMs, leading to the production of IL-6. rVpr-induced IL-6 production depended on the activation of NF-κB and MAPK signaling and the phosphorylation of C/EBP-β. Moreover, we found that rVpr-induced oxidative stress caused the formation of OxPC, and pretreatment with DLH3, a mAb against OxPC, blocked rVpr-induced IL-6 production and the phosphorylation of C/EBP-β. These data indicate that IL-6 production is initiated by the formation of OxPC generated by the effects of rVpr-induced oxidative stress. Varin et al. [36] reported that a synthetic Vpr peptide activated AP-1, JNK, and NF-κB signaling, resulting in increased viral replication; however, the molecular mechanism involved remains to be clarified. Our current work provides an explanation for the activation of these cellular responses by Vpr-induced oxidative stress. We hypothesize that OxPC, as the most upstream event, extracellularly activates TLR4-mediated signaling. This notion is supported by previous data reported by Imai et al. [27] that TLR4 signaling is activated by acid challenge or treatment with H5N1 in mouse lungs via OxPC. They detected OxPC generated in bronchoalveolar lavage in affected mouse lungs and showed that its activity was blocked by a mAb against OxPC. However, our blocking experiments with DLH3 cannot exclude the possibility that the formation of OxPC and activation of TLR4-mediated cellular signals are required independently for Vpr-induced IL-6 production. Here, we showed that OxPC-triggered cellular signals were dependent on MyD88, whereas those induced by SARS-CoV were shown to be MyD88-independent [27]. These discrepant observations may have been a result of differences in the experimental conditions applied; we used human monocytes/macrophages, whereas Imai et al. [27] used rodent cells.

ROS are likely generated as a result of the mitochondrial dysfunction caused by Vpr. With regard to the mechanism of mitochondrial dysfunction, it has been shown that Vpr binds ANT, a member of the permeability transition pore complex [39], and disrupts the MMP [17]. The domain of Vpr involved in mitochondrial toxicity has been identified as the region encompassing aa 72–83, and arginine residues at positions 73, 77, and 80 (R73, R77, and R80) were defined as being critical for the interaction with ANT [39]. We showed previously that a mutant rVpr protein with alanines in place of the three arginines lacked the ability to impair the MMP and neurite outgrowth [17]. Additionally, a mutant virus carrying Vpr, altered at R77, was detected in patients who were HIV-1-positive and diagnosed as long-term nonprogressors [40], suggesting that the Vpr-induced killing activity of T cells might be linked directly to the clinical outcome of these individuals.

Our finding that exogenously added rVpr reactivated viral reproduction in latently infected cells will broaden our understanding of the pathophysiology in HIV-1-positive patients. HAART dramatically improves the prognosis of HIV-1-positive patients; unfortunately, however, it was concluded that complete eradication of the virus by the chemotherapeutics currently available would take more than 60 years [41]. Such observations underscore the importance of preventing new episodes of viral infection or restraining viral production from latent reservoirs. Vpr has been postulated to function as a necessary factor in the primary infection of resting macrophages and to enhance viral reproduction following latency. As reported previously [13], Vpr is present in the plasma of HIV-1-positive patients, and we ascertained that rVpr added exogenously at the nM level, which is comparable with the level observed in patient plasma, reproducibly reactivated viral production from latency via IL-6 production. Although autoantibodies to Vpr [42] might neutralize its activity, we suggest the importance of monitoring patient plasma Vpr levels in the context of the clinical course. Our results provide a rationale for the development of novel anti-AIDS therapeutics against Vpr.

REFERENCES

1. Palella, F. J., Delaney, K. M., Moorman, A. C., Loveless, M. O., Fuhrer, J., Satten, G. A., Aschman, D. J., Holmberg, S. D. (1998) Declining morbidity and mortality among patients with advanced human immunodeficiency virus infection. HIV Outpatient Study Investigators. *N. Engl. J. Med.* **338**, 853–860.
2. Siliciano, J. D., Kajdas, J., Finzi, D., Quinn, T. C., Chadwick, K., Margolick, J. B., Kovacs, C., Gange, S. J., Siliciano, R. F. (2003) Long-term follow-up studies confirm the stability of the latent reservoir for HIV-1 in resting CD4+ T cells. *Nat. Med.* **9**, 727–728.
3. Finzi, D., Hermankova, M., Pierson, T., Carruth, L. M., Buck, C., Chaisson, R. E., Quinn, T. C., Chadwick, K., Margolick, J., Brookmeyer, R., Gallant, J., Markowitz, M., Ho, D. D., Richman, D. D., Siliciano, R. F. (1997) Identification of a reservoir for HIV-1 in patients on highly active antiretroviral therapy. *Science* **278**, 1295–1300.
4. Folks, T. M., Justement, J., Kinter, A., Dinarello, C. A., Fauci, A. S. (1987) Cytokine-induced expression of HIV-1 in a chronically infected promonocyte cell line. *Science* **238**, 800–802.

5. Koyanagi, Y. O'Brien, W. A., Zhao, J. Q., Golde, D. W., Gasson, J. C., Chen, I. S. (1988) Cytokines alter production of HIV-1 from primary mononuclear phagocytes. *Science* **241,** 1673–1675.
6. Valerie, K., Delers, A., Bruck, C., Thiriart, C., Rosenberg, H., Debouck, C., Rosenberg, M. (1988) Activation of human immunodeficiency virus type 1 by DNA damage in human cells. *Nature* **333,** 78–81.
7. Gendelman, H. E., Orenstein, J. M., Baca, L. M., Weiser, B., Burger, H., Kalter, D. C., Meltzer, M. S. (1989) The macrophage in the persistence and pathogenesis of HIV infection. *AIDS* **3,** 475–495.
8. Lambotte, O., Taoufik, Y., Goër, M. G., Wallon, C., Goujard, C., Delfraissy, J. F. (2000) Detection of infectious HIV in circulating monocytes from patients on prolonged highly active antiretroviral therapy. *J. Acquir. Immune Defic. Syndr.* **23,** 114–119.
9. Olafsson, K., Smith, M. S., Marshburn, P., Carter, S. G., Haskill, S. (1991) Variation of HIV infectibility of macrophages as a function of donor, stage of differentiation, and site of origin. *J. Acquir. Immune Defic. Syndr.* **4,** 154–164.
10. Vodicka, M. A., Koepp, D. M., Silver, P. A., Emerman, M. (1998) HIV-1 Vpr interacts with the nuclear transport pathway to promote macrophage infection. *Genes Dev.* **12,** 175–185.
11. Levy, D. N., Refaeli, Y., MacGregor, R. R., Weiner, D. B. (1994) Serum Vpr regulates productive infection and latency of human immunodeficiency virus type 1. *Proc. Natl. Acad. Sci. USA* **91,** 10873–10877.
12. Levy, D. N., Refaeli, Y., Weiner, D. B. (1995) Extracellular Vpr protein increases cellular permissiveness to human immunodeficiency virus replication and reactivates virus from latency. *J. Virol.* **69,** 1243–1252.
13. Hoshino, S., Sun, B., Konishi, M., Shimura, M., Segawa, T., Hagiwara, Y., Koyanagi, Y., Iwamoto, A., Mimaya, J., Terunuma, H., Kano, S., Ishizaka, Y. (2007) Vpr in plasma of HIV type 1-positive patients is correlated with the HIV type 1 RNA titers. *AIDS Res. Hum. Retroviruses* **23,** 391–397.
14. Malim, M. H., Emerman, M. (2008) HIV-1 accessory proteins—ensuring viral survival in a hostile environment. *Cell Host Microbe* **3,** 388–398.
15. Ayyavoo, V., Mahboubi, A., Mahalingam, S., Ramalingam, R., Kudchodkar, S., Williams, W. V., Green, D. R., Weiner, D. B. (1997) HIV-1 Vpr suppresses immune activation and apoptosis through regulation of nuclear factor κ B. *Nat. Med.* **3,** 1117–1123.
16. Patel, C. A., Mukhtar, M., Pomerantz, R. J. (2000) Human immunodeficiency virus type 1 Vpr induces apoptosis in human neuronal cells. *J. Virol.* **74,** 9717–9726.
17. Kitayama, H., Miura, Y., Ando, Y., Hoshino, S., Ishizaka, Y., Koyanagi, Y. (2008) Human immunodeficiency virus type 1 Vpr inhibits axonal outgrowth through induction of mitochondrial dysfunction. *J. Virol.* **82,** 2528–2542.
18. Wiley, C. A., Achim, C. (1994) Human immunodeficiency virus encephalitis is the pathological correlate of dementia in acquired immunodeficiency syndrome. *Ann. Neurol.* **36,** 673–676.
19. Deshmane, S. L., Mukerjee, R., Fan, S., Valle, L. D., Michiels, C., Sweet, T., Rom, I., Khalili, K., Rappaport, J., Amini, S., Sawaya, B. E. (2009) Activation of the oxidative stress pathway by HIV-1 Vpr leads to induction of hypoxia-inducible factor 1α expression. *J. Biol. Chem.* **284,** 11364–11373.
20. Roc, A. C., Ances, B. M., Chawla, S., Korczykowski, M., Wolf, R. L., Kolson, D. L., Detre, J. A., Poptani, H. (2007) Detection of human immunodeficiency virus induced inflammation and oxidative stress in lenticular nuclei with magnetic resonance spectroscopy despite antiretroviral therapy. *Arch. Neurol.* **64,** 1249–1257.
21. Nath, A., Schiess, N., Venkatesan, A., Rumbaugh, J., Sacktor, N., McArthur, J. (2008) Evolution of HIV dementia with HIV infection. *Int. Rev. Psychiatry* **20,** 25–31.
22. Akira, S., Uematsu, S., Takeuchi, O. (2006) Pathogen recognition and innate immunity. *Cell* **124,** 783–801.
23. Uematsu, S., Akira, S. (2006) Toll-like receptors and innate immunity. *J. Mol. Med.* **84,** 712–725.
24. Kawai, T., Akira, S. (2008) Toll-like receptor and RIG-I-like receptor signaling. *Ann. N. Y. Acad. Sci.* **1143,** 1–20.
25. Zarubin, T., Han, J. (2005) Activation and signaling of the p38 MAP kinase pathway. *Cell Res.* **15,** 11–18.
26. Philpott, K. L., Facci, L. (2008) MAP kinase pathways in neuronal cell death. *CNS Neurol. Disord. Drug Targets* **7,** 83–97.
27. Imai, Y., Kuba, K., Neely, G. G., Yaghubian-Malhami, R., Perkmann, T., Loo, G. V., Ermolaeva, M., Veldhuizen, R., Leung, Y. H., Wang, H., Liu, H., Sun, Y., Pasparakis, M., Kopf, M., Mech, C., Bavari, S., Peiris, J. S., Slutsky, A. S., Akira, S., Hultqvist, M., Holmdahl, R., Nicholls, J., Jiang, C., Binder, C. J., Penninger, J. M. (2008) Identification of oxidative stress and Toll-like receptor 4 signaling as a key pathway of acute lung injury. *Cell* **133,** 235–249.
28. Rahangdale, S., Yeh, S. Y., Malhotra, A., Veves, A. (2009) Therapeutic interventions and oxidative stress in diabetes. *Front. Biosci.* **14,** 192–209.
29. Praticò, D. (2008) Evidence of oxidative stress in Alzheimer's disease brain and antioxidant therapy: lights and shadows. *Ann. N. Y. Acad. Sci.* **1147,** 70–78.
30. Zhou, C., Huang, Y., Przedborski, S. (2008) Oxidative stress in Parkinson's disease: a mechanism of pathogenic and therapeutic significance. *Ann. N. Y. Acad. Sci.* **1147,** 93–104.
31. Shimura, M., Osawa, Y., Yuo, A., Hatake, K., Takaku, F., Ishizaka, Y. (2000) Oxidative stress as a necessary factor in room temperature-induced apoptosis of HL-60 cells. *J. Leukoc. Biol.* **68,** 87–96.
32. Eickelberg, O., Pansky, A., Mussmann, R., Bihl, M., Tamm, M., Hildebrand, P., Perruchoud, A. P., Roth, M. (1999) Transforming growth factor-β1 induces interleukin-6 expression via activating protein-1 consisting of JunD homodimers in primary human lung fibroblasts. *J. Biol. Chem.* **274,** 12933–12938.
33. Itabe, H., Takeshima, E., Iwasaki, H., Kimura, J., Yoshida, Y., Imanaka, T., Takano, T. (1994) A monoclonal antibody against oxidized lipoprotein recognizes foam cells in atherosclerotic lesions. Complex formation of oxidized phosphatidylcholines and polypeptides. *J. Biol. Chem.* **269,** 15274–15279.
34. Itabe, H., Yamamoto, H., Suzuki, M., Kawai, Y., Nakagawa, Y., Suzuki, A., Imanaka, T., Takano, T. (1996) Oxidized phosphatidylcholines that modify proteins. Analysis by monoclonal antibody against oxidized low density lipoprotein. *J. Biol. Chem.* **271,** 33208–33217.
35. Mitsuzawa, H., Nishitani, C., Hyakushima, N., Shimizu, T., Sano, H., Matsushima, N., Fukase, K., Kuroki, Y. (2006) Recombinant soluble forms of extracellular TLR4 domain and MD-2 inhibit lipopolysaccharide binding on cell surface and dampen lipopolysaccharide-induced pulmonary inflammation in mice. *J. Immunol.* **177,** 8133–8139.
36. Varin, A., Decrion, A. Z., Sabbah, E., Quivy, V., Sire, J., Van, L. C., Roques, B. P., Aggarwal, B. B., Herbein, G. (2005) Synthetic Vpr protein activates activator protein-1, c-Jun N-terminal kinase, and NF-κB and stimulates HIV-1 transcription in promonocytic cells and primary macrophages. *J. Biol. Chem.* **280,** 42557–42567.
37. Alpert, D., Vilcek, J. (2000) Inhibition of IκB kinase activity by sodium salicylate in vitro does not reflect its inhibitory mechanism in intact cells. *J. Biol. Chem.* **275,** 10925–10929.
38. Shimura, M., Tanaka, Y., Nakamura, S., Minemoto, Y., Yamashita, K., Hatake, K., Takaku, F., Ishizaka, Y. (1999) Micronuclei formation and aneuploidy induced by Vpr, an accessory gene of human immunodeficiency virus type 1. *FASEB J.* **13,** 621–637.
39. Jacotot, E., Ravagnan, L., Loeffler, M., Ferri, K. F., Vieira, H. L., Zamzami, N., Costantini, P., Druillennec, S., Hoebeke, J., Briand, J. P., Irinopoulou, T., Daugas, E., Susin, S. A., Cointe, D., Xie, Z. H., Reed, J. C., Roques, B. P., Kroemer, G. (2000) The HIV-1 viral protein R induces apoptosis via a direct effect on the mitochondrial permeability transition pore. *J. Exp. Med.* **191,** 33–46.
40. Lum, J. J., Cohen, O. J., Nie, Z., Weaver, J. G., Gomez, T. S., Yao, X-J., Lynch, D., Pilon, A. A., Hawley, N., Kim, J. E., Chen, Z., Montpetit, M., Sanchez-Dardon, J., Cohen, E. A., Badley, A. D. (2003) Vpr R77Q is associated with long-term nonprogressive HIV infection and impaired induction of apoptosis. *J. Clin. Invest.* **111,** 1547–1554.
41. Finzi, D., Blankson, J., Siliciano, J. D., Margolick, J. B., Chadwick, K., Pierson, T., Smith, K., Lisziewicz, J., Lori, F., Flexner, C., Quinn T. C., Chaisson R. E., Rosenberg E., Walker B., Gange S., Gallant J., Siliciano R. F. (1999) Latent infection of CD4+ T cells provides a mechanism for lifelong persistence of HIV-1, even in patients on effective combination therapy. *Nat. Med.* **5,** 512–517.
42. Reiss, P., Lange, J. M., de Ronde, A., de Wolf, F., Dekker, J., Danner, S. A., Debouck, C., Goudsmit, J. (1990) Antibody response to viral proteins U (vpu) and R (vpr) in HIV-1-infected individuals. *J. Acquir. Immune Defic. Syndr.* **3,** 115–122.

KEY WORDS:
oxidative stress · oxidized phosphatidylcholine

Vaccine 28S (2010) B32–B37

Contents lists available at ScienceDirect

Vaccine

journal homepage: www.elsevier.com/locate/vaccine

Dynamics of memory and naïve CD8$^+$ T lymphocytes in humanized NOD/SCID/IL-2Rγ^{null} mice infected with CCR5-tropic HIV-1

Kei Sato[a,1], Chuanyi Nie[a,1], Naoko Misawa[a,1], Yuetsu Tanaka[b], Mamoru Ito[c], Yoshio Koyanagi[a,*]

[a] Laboratory of Viral Pathogenesis, Institute for Virus Research, Kyoto University, 53 Shogoinkawara-cho, Sakyo-ku, Kyoto, Kyoto 606-8507, Japan
[b] Department of Immunology, Graduate School of Medicine, University of the Ryukyus, Nishihara, Okinawa 903-0125, Japan
[c] Central Institute for Experimental Animals, Kawasaki, Kanagawa 216-0001, Japan

ARTICLE INFO

Article history:
Received 15 May 2009
Received in revised form 3 August 2009
Accepted 29 October 2009

Keywords:
HIV-1
Humanized mice
Immunopathogenesis

ABSTRACT

Creating a novel small animal model of HIV-1 infection that can support long-term systemic HIV-1 infection and produce HIV-1-specific immune response has a great benefit for studying HIV-1 pathogenesis *in vivo*. In the present study, we have generated a humanized mouse, NOG-hCD34 mouse, by transplanting newborn NOD/SCID/IL-2Rγ^{null} mice with human hematopoietic stem cells through hepatic injection. These mice were infected with a CCR5-tropic HIV-1 and were analyzed for plasma viral load, changes in peripheral blood T lymphocytes, and HIV-1-specific antibody production. High level of viral replication, increase in effector/memory CD8$^+$ T lymphocytes, class-switching to IgG, and production of HIV-1-specific IgGs were observed. Our findings suggest that NOG-hCD34 mice may have a wide variety of application in HIV-1 research.

1. Introduction

Human immunodeficiency virus type 1 (HIV-1) is a retrovirus that causes immunodeficiency exclusively in human [1]. The inability of HIV-1 to cause immunodeficiency in other animals has made authentic investigations in live animals extremely difficult, thus preventing the advancement of our understanding on the pathogenesis of HIV-1 *in vivo*.

Tremendous efforts have been made to generate a cost-efficient and readily accessible small animal model that can be used to investigate the pathogenesis of HIV-1, to test the effectiveness of anti-HIV-1 drug candidates, and to test HIV-1 vaccines *in vivo* [2–4]. Initial successful attempts included C.B17-severe combined immunodeficient (SCID) mice transplanted under the kidney capsule with fragments of human fetal thymus, lymph node, and human hematopoietic cells-containing human fetal liver (Thy/Liv SCID-hu mice) [5,6] or in the peritoneal space with human peripheral blood lymphocytes (hu-PBL-SCID mice) [7]. Thy/Liv SCID-hu mice are able to support *de novo* generation of human T lymphocytes and thus are useful for the studies of HIV-1 intrathymic infection and hematopoiesis suppression [8]. However, HIV-1 infection in Thy/Liv SCID-hu mice is restricted to the transplanted organ, and Thy/Liv SCID-hu mice are not able to support multilineage differentiation of human hematopoietic cells [9]. On the other hand, hu-PBL-SCID mice are able to reproduce high level of systemic HIV-1 infection, but the lack of on-going *de novo* human hematopoiesis and the short life span limited their application [10].

In order to improve a small animal model for the testing of anti-HIV-1 therapy and HIV-1 vaccines, HIV-1 infection must be sustained and immune response against HIV-1 must be generated within the animal. We have previously created a novel non-obese diabetic/severe combined immunodeficient (NOD/SCID) interleukin-2 receptor gamma chain (IL-2Rγ) knockout (NOD/SCID/IL-2Rγ^{null}; NOG) mouse strain, which lacks intrinsic T and B lymphocytes and functional natural killer cells [11]. NOG mice have been shown to be feasible for transplantation of human CD34$^+$ hematopoietic stem cells (hHSCs) and for supporting the differentiation of human T lymphocytes [11–13]. In adult NOG mice transplanted with hHSCs, it has been found that the CD34$^+$ cells successfully differentiated into human T and B lymphocytes, monocytes/macrophages, natural killer (NK) cells, as well as plasmacytoid and myeloid dendritic cells (DCs), and that these human cells were maintained for more than 150 days [12,14]. It was also reported that adult NOG mice transplanted with hHSCs supported HIV-1 infection for more than 3 months and produced HIV-1-specific antibodies [12]. These findings suggested that hHSCs-transplanted NOG mouse would be a useful animal model to study HIV-1 infection. However, whether hHSCs-transplanted NOG mice can mount a CD8$^+$ T lymphocyte-mediated immune response against HIV-1 has not been investigated yet.

In this paper, we generated humanized mice by transplanting newborn NOG mice with hHSCs via hepatic injection (NOG-hCD34

* Corresponding author. Tel.: +81 75 751 4811.
E-mail address: ykoyanag@virus.kyoto-u.ac.jp (Y. Koyanagi).
[1] These authors contributed equally to this work.

0264-410X/$ – see front matter © 2009 Elsevier Ltd. All rights reserved.
doi:10.1016/j.vaccine.2009.10.154

mice), because it has been suggested that transplantation of cord blood (CB)-derived hHSCs into newborn mice results in better immune reconstitution [15,16]. Our humanized mice supported high level of HIV-1 replication. We observed that *de novo* generated $CD8^+$ T lymphocytes gained effector/memory phenotype in response to HIV-1 infection and massively proliferated. Based on our findings, we discuss the possibility of the application of NOG-CD34 mice, particularly those transplanted during the neonatal period, for HIV-1 research.

2. Material and methods

2.1. Mice

NOD/SCID/IL-2Rγ^{null} mice (NOG mice [11]) were obtained from the Central Institute for Experimental Animals (Kawasaki, Japan). The mice were maintained under specific pathogen-free conditions and were handled in accordance with the Regulation on Animal Experimentation at Kyoto University.

2.2. Purification and transplantation of CB-derived hHSCs

The purification and transplantation of CB-derived hHSCs was conducted as described previously with some modification [14–16]. Fresh human CB was obtained with parent written informed consent from healthy full-term newborns and CD34 MicroBead Kit (Miltenyi Biotec, Auburn, CA) was used according to the manufacturer's instructions. $CD34^+$ cells ($5–12 \times 10^4$) were intrahepatically injected into newborn mice of ages between 0 and 2 days after total radiation of 10 cGy per mouse in MBR-1520 X-ray irradiator (Hitachi Medico, Tokyo, Japan).

2.3. HIV-1 infection

NOG-hCD34 mice were injected intraperitoneally with RPMI1640 or 1×10^5 50% tissue culture infective doses ($TCID_{50}$) of HIV-$1_{JR\text{-}CSF}$ [17] between 12 and 13 weeks post-transplantation. HIV-$1_{JR\text{-}CSF}$ solution was prepared and titrated previously described [18,19].

2.4. Quantification of HIV-1 RNA in plasma

The quantification of HIV-1 RNA in the plasma of the infected mice was routinely carried out using Amplicor HIV-1 monitor v1.5 according to the manufacturer's protocol (Roche Diagnostics, Mannheim, Germany).

2.5. Peripheral blood collection and isolation of nucleated cells from organs

Peripheral blood (PB) was routinely collected from NOG-hCD34 mice as described previously [16]. Red blood cells in the PB were lysed with 1× BD Lysis Buffer (BD Pharmingen, San Diego, CA). Mononuclear cells from bone marrow (BM), thymus, spleen, and lymph nodes were collected as described previously [16], and single cell suspensions were used for flow cytometric analysis or stored at −80 °C until use.

2.6. Flow cytometry

Flow cytometric analysis was performed with some modifications to the protocol previously described [15,19]. Following mouse monoclonal antibodies (mMAbs) and reagents were used: FITC-conjugated anti-CD19 (Dako, Tokyo, Japan), anti-CD8 (Dako), anti-CD4 (eBioscience, San Diego, CA), and anti-CD14 (Miltenyi Biotec) mMAbs, PE-conjugated anti-CD3 (Dako), anti-CD4 (Dako), anti-CCR5 (BD Pharmingen), and anti-CD34 (Miltenyi Biotec) mMAbs, biotinylated anti-CD45 (eBioscience) and anti-CD45RA (BD Pharmingen) mMAbs, PerCP-conjugated streptavidin (BD Immunocytometry systems, San Jose, CA), and FcR blocker (Myltenyi Biotec). Each antibody was controlled with appropriate isotype IgGs (Dako). Following first incubation, the cells were washed and further incubated with PerCP-conjugated streptavidin if needed. For p24 staining, the cells were permeabilized and fixed by treatment with BD Cytoperm/Cytofix solution (BD Pharmingen) and were stained with FITC-conjugated rat anti-HIV-1 p24 MAb (clone 2C2) [20] for 30 min at 4 °C in 1× BD PermWash buffer (BD Pharmingen). Data collection was performed on BD FACSCan (BD Biosciences, San Jose, CA), and the obtained data was analyzed with CellQuest software (BD Biosciences).

2.7. Detection of reactive human IgG against HIV-1 antigens

Plasma was collected from 1 mock-infected and 7 HIV-$1_{JR\text{-}CSF}$-infected NOG-hCD34 mice upon the time of sacrifice. The presence of human IgGs against HIV-1 antigens in the collected plasma was examined by using a New Lav Blot 1 kit (Bio-Rad, Hercules, CA) according to the manufacturer's protocol.

2.8. Statistic analysis

Significant differences were determined by Student's *t* test or paired *t* test. *P* value less than 0.05 was considered significantly different.

3. Results

3.1. Reconstruction of human leukocytes in NOG-hCD34 mice

We first investigated the ability of newborn NOG mice transplanted with hHSCs to support human hematopoiesis. These mice are referred to as NOG-hCD34 mice. The flow cytometric analyses revealed that substantial percentages of human $CD45^+$ leukocytes including $CD3^+$ T lymphocytes and $CD19^+$ B lymphocytes already presented in the PB of 13-week-old mice and were stably maintained for at least 31 weeks (Table 1). $CD3^+$ T lymphocytes in the PB of these mice were singly positive for either CD4 or CD8 (Table 1). In the thymi of NOG-hCD34 mice, $CD45^+$ cells were detected in great abundance, which were predominantly CD4CD8 double positive cells (Table 1). In the BM sampled from femurs of NOG-hCD34 mice, we found large number of human $CD45^+$ leukocytes including $CD34^+$ hematopoietic cells, $CD3^+$ T lymphocytes, $CD19^+$ B lymphocytes, and $CD14^+$ monocytes (Table 1). In the secondary lymphoid organs of the mice, large populations of human leukocytes including $CD3^+$ and $CD19^+$ lymphocytes were detected (Table 1). In addition, we also found significant number of $CCR5^+CD4^+$ T lymphocytes, which are the target cells for CCR5-tropic HIV-1, in the spleen of NOG-hCD34 mice ($7.5 \pm 2.6\%$ in splenic mononuclear cells).

3.2. Significant and persistent viremia in PB of NOG-hCD34 mice

NOG-hCD34 mice between 12 and 13-week old were infected with HIV-$1_{JR\text{-}CSF}$ (1×10^5 $TCID_{50}$/mouse). HIV-$1_{JR\text{-}CSF}$ uses the chemokine receptor CCR5 as the co-receptor for its infection [21]. In the plasma of HIV-$1_{JR\text{-}CSF}$-infected NOG-hCD34 mice, high levels of HIV-1 were detected starting 2–3 weeks post-infection (wpi) ($1.28 \pm 0.65 \times 10^5$ copies/ml) and were maintained throughout the period of investigation (Fig. 1A). Of note, the plasma RNA levels were comparable to that found in patients with acute HIV-1 infection [22]. We also confirmed that HIV-1 RNA was undetectable in the plasma of mock-infected mice (<1600 copies/ml). In addition to

Table 1
Reconstitution of human multilineage leukocytes in NOG-hCD34 mice[a,b].

Linage marker[c]	CD45$^+$	CD3$^+$	CD19$^+$	CD4$^+$	CD8$^+$	CD14$^+$	CD34$^+$
PB (12–13-week old)	34.9 ± 11.3	10.2 ± 6.9	17.5 ± 6.3	4.7 ± 2.9	5.2 ± 3.3	n.a.[f]	n.a.
PB (28–31-week old)	33.3 ± 14.5	22.4 ± 6.8	8.7 ± 9.1	14.0 ± 6.2	5.4 ± 2.3	0.2 ± 0.2	n.a.
BM[d]	43.2 ± 20.8	7.8 ± 5.7	27.2 ± 24.6	n.a.	n.a.	2.7 ± 3.2	5.4 ± 3.9
Spleen[d]	75.9 ± 16.4	42.9 ± 22.9	25.6 ± 12.3	26.3 ± 10.6	11.5 ± 8.0	n.a.	n.a.
Lymph nodes[d]	94.8 ± 5.1	82.2 ± 8.7	8.0 ± 4.2	n.a.	n.a.	n.a.	n.a.

Linage marker[e]	CD45$^+$	CD4SP	CD8SP	DP	DN
Thymus[d]	98.5 ± 0.4	12.6 ± 7.7	6.5 ± 4.9	76.3 ± 20.9	10.8 ± 10.6

[a] Each population of human leukocytes in NOG-hCD34 mice (n = 4–8) was analyzed by flow cytometry as described in Section 2.
[b] Average percentage of each linage marker positive cell in whole mononuclear cells is shown with standard deviation.
[c] Each linage marker indicates followings: CD45, pan leukocytes; CD3, T lymphocytes; CD19, B lymphocytes; CD14, monocytes; CD34, hematopoietic cells.
[d] Tissues were collected between 28 and 44 weeks old as described in Section 2.
[e] SP, single positive; DP, CD4CD8 double positive; DN, CD4CD8 double negative.
[f] Not analyzed.

the detection of viral RNA in plasma (Fig. 1A), we detected the cells positive for an HIV-1 antigen, p24, in the spleen of the infected mice (Fig. 1B). These results indicate that HIV-$1_{JR\text{-}CSF}$ was sufficiently replicated in NOG-hCD34 mice.

The PB samples of HIV-$1_{JR\text{-}CSF}$-infected and mock-infected NOG-hCD34 mice were periodically collected and human lymphocytes were sequentially analyzed by flow cytometry. We observed that peripheral CD4$^+$ to CD8$^+$ ratio of HIV-$1_{JR\text{-}CSF}$-infected mice was

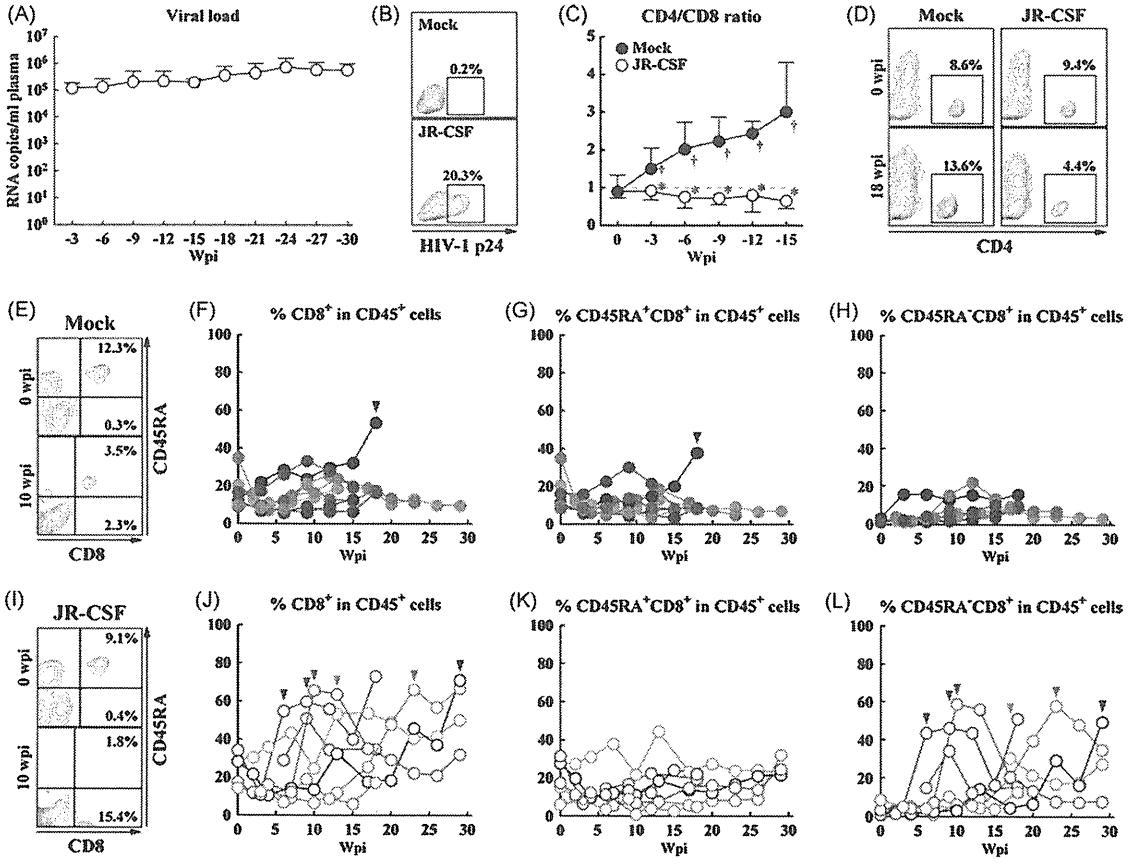

Fig. 1. Immunopathological analyses on CCR5-tropic HIV-1-infected NOG-hCD34 mice. NOG-hCD34 mice were intraperitoneally inoculated with RPMI1640 (for mock infection, filled circles, n = 8) or HIV-$1_{JR\text{-}CSF}$ (1×10^5 $TCID_{50}$/mouse, opened circles, n = 7) between 12 and 13-week old. (A) The longitudinal analysis on the plasma viral load of HIV-$1_{JR\text{-}CSF}$-infected mice. Plasma was routinely collected and HIV-1 RNA was quantified as described in Section 2. (B) Detection of HIV-1 antigen-expressing cells. Splenic mononuclear cells of mock-infected (top) and HIV-$1_{JR\text{-}CSF}$-infected (bottom) mice were stained with an anti-HIV-1 p24 antibody and analyzed by flow cytometry. A representative results are shown. The percentages in plots indicate the percentage of p24-positive cells in splenic whole mononuclear cells. (C–L) The longitudinal analyses in the PB of mock-infected and HIV-$1_{JR\text{-}CSF}$-infected mice. PB was routinely collected and longitudinally analyzed by flow cytometry. (C) CD4/CD8 ratio in the PB. Broken line in gray indicates CD4/CD8 ratio = 1. (D) Representative profiles of CD4$^+$ T lymphocytes in the PB. The results in the PB of mock-infected (left) and HIV-$1_{JR\text{-}CSF}$-infected (right) mice at 0 wpi (top) and 18 wpi (bottom) are shown. The percentages in plots indicate the percentage of CD4-positive cells in whole mononuclear cells. (E–H) The percentages of whole CD8$^+$ (F and J), naïve CD45RA$^+$CD8$^+$ (G and K), and memory CD45RA$^-$CD8$^+$ (H and L) T lymphocytes in the PB of mock-infected (F–H) and HIV-$1_{JR\text{-}CSF}$-infected (J–L) mice are shown. (E and I) Representative profiles of naïve and memory CD8$^+$ T lymphocytes in the PB. The results in the PB of mock-infected (E) and HIV-$1_{JR\text{-}CSF}$-infected (I) mice at 0 wpi (top) and 10 wpi (bottom) are shown. The percentages in each quadrant indicate the percentages of CD8$^+$CD45RA$^+$ naïve cells (right upper) and CD8$^+$CD45RA$^-$ memory cells (right lower) in whole mononuclear cells. In panels A and C, the data are assigned into periodic groups (0, 1–3, 4–6, 7–9, 10–12, 13–15, 16–18, 19–21, 22–24, 25–27, and 28–30 wpi). Error bars in panels A and C represent standard deviations. Arrowheads in panels F, G, J, and L indicate distinctive peaks or increases in the percentages of CD8$^+$ T lymphocytes or their subsets. Asterisks represent statistical differences (P < 0.05 by Student's t test) versus the values of mock-infected mice at the same time point, and daggers represent statistical differences (P < 0.05 by paired t test) versus the value at 0 wpi.

constantly lower than that of the mock-infected mice (Fig. 1C). Moreover, the percentage of peripheral $CD4^+$ T lymphocytes in both human $CD45^+$ cells and whole mononuclear cells of mock-infected mice mildly increased, while this increase was not observed in HIV-$1_{JR\text{-}CSF}$-infected mice (Fig. 1D).

3.3. Proliferation of memory $CD8^+$ T lymphocytes in CCR5-tropic HIV-1-infected NOG-hCD34 mice

We also longitudinally analyzed on the percentages of $CD8^+$ T lymphocytes within human $CD45^+$ cells in the PB of mock-infected and HIV-$1_{JR\text{-}CSF}$-infected mice (Fig. 1E–L). $CD8^+$ T lymphocytes were further distinguished into memory and naïve populations on the basis of naïve T-cell marker CD45RA. In the mock-infected mice, the percentages of whole $CD8^+$ (Fig. 1F), $CD45RA^+CD8^+$ naïve (Fig. 1G), and memory $CD45RA^-CD8^+$ (Fig. 1H) T lymphocytes stayed consistent throughout the investigation with one exception that displayed increase in the percentage of $CD8^+$ T lymphocytes (Fig. 1F). This increase was attributed to an occasional increase in $CD45RA^+$ subset of $CD8^+$ T lymphocytes (Fig. 1G, arrowhead). In contrast, in 6 out of the 7 HIV-$1_{JR\text{-}CSF}$-infected mice, the percentages of whole $CD8^+$ and memory $CD45RA^-CD8^+$ T lymphocytes drastically increased after infection displaying distinctive peaks (Fig. 1J and L with arrowheads. A representative result is shown in Fig. 1I), while the percentages of naïve $CD45RA^+CD8^+$ T lymphocytes stayed quite stable (Fig. 1K). The peaks in the percentage of $CD45RA^-CD8^+$ T lymphocytes directly correlated to those in the percentage of $CD8^+$ T lymphocytes (Fig. 1J and L), indicating that the increase in the $CD8^+$ T lymphocyte population was caused by the increase in the $CD45RA^-$ memory subset.

3.4. Production of antibodies against HIV-1 antigens in CCR5-tropic HIV-1-infected NOG-hCD34 mice

In addition to the proliferative response of memory $CD8^+$ T lymphocytes in HIV-$1_{JR\text{-}CSF}$-infected mice, we found successful differentiation of human $CD19^+$ B lymphocytes in NOG-hCD34 mice (Table 1). To examine whether human antibody response against HIV-1 antigens was induced in the infected mice, we tested the plasma of a mock-infected and 7 HIV-$1_{JR\text{-}CSF}$-infected mice by Western blotting (Fig. 2), which has been clinically utilized for the definitive diagnosis of HIV-1 infection. In the plasma of all NOG-hCD34 mice, human IgG was detected (Fig. 2, lanes 2–4 and not shown), indicating that class-switching of immunoglobulin from IgM to IgG in human B cells occurred. However, we only detected human IgG that reacts with HIV-1 gp41 in the plasma of 2 infected mice (Fig. 2, lanes 3 and 4 with arrowheads). This suggests that generation of humoral immune response against HIV-1 may be limited in the infected mice.

4. Discussion

Adult NOG mice have been shown to be able to effectively support *de novo* generation of multilineage human immune cells when transplanted with hHSCs [11–13]. In the present study, we generated NOG-hCD34 mice, which are neonatal NOG mice transplanted with CB-derived hHSCs. These mice produced human T lymphocytes, B lymphocytes, and monocytes, and sustained steady human hematopoiesis for at least 31 weeks (217 days). They were susceptible to infection by HIV-$1_{JR\text{-}CSF}$, and showed high level of persistent viral replication. Furthermore, in addition to the production of HIV-1-specific IgG, human $CD8^+$ T lymphocytes proliferated in HIV-$1_{JR\text{-}CSF}$-infected mice. These suggest that NOG-hCD34 mice have the potential to be of valuable tool for the study of HIV-1 infection *in vivo*.

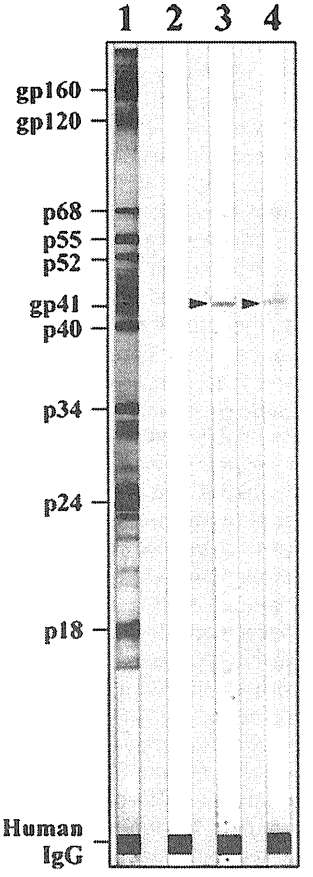

Fig. 2. Production of human IgG and antibodies against HIV-1 antigens in the plasma of CCR5-tropic HIV-1-infected NOG-hCD34 mice. Plasmas were collected from a mock-infected and 7 HIV-$1_{JR\text{-}CSF}$-infected NOG-hCD34 mice upon sacrifice and were examined for the presence of human IgG against HIV-1 antigens as described in Section 2. Representative results from serum of a human HIV-1 positive patient (positive control) (lane 1), and plasmas sampled from a mock-infected (lane 2) and 2 HIV-$1_{JR\text{-}CSF}$-infected (lanes 3 and 4) mice are shown. Arrowheads indicate bands showing the presence of human IgG that reacted with HIV-1 gp41.

Classical xenotransplantation of hHSCs in mice used to be unsuccessful in producing *de novo* generated T lymphocytes, because immune cells in recipient mice interfered with hematopoiesis of the transplanted cells [23]. Human T lymphocytes failed to develop even in NOD/SCID mice, a strain of mice considered to have one of the most underdeveloped immune system [24]. The treatment of NOD/SCID mice with anti-NK cell antibody prior to xenotransplantation enhanced the engraftment efficiency, suggesting that NK cells were important mediators of graft failure in NOD/SCID mice [24]. Subsequently, highly immunodeficient strains of mice such as NOG mice and Rag2$^{-/-}\gamma_c^{-/-}$ mice were generated and were found to be much better recipients for human grafts [11,15,25]. NOG mice, which are NOD/SCID mice with null mutation at the IL-2Rγ gene, were completely defective in NK cell function [11]. NOG-hCD34 mice supported the differentiation of human leukocytes including T lymphocytes from engrafted hHSCs, and they were shown to support long-term productive infection by HIV-1 [11–15]. In adult NOG mice transplanted with hHSCs, HIV-1 infection resulted in production of HIV-1-specific antibody response [12]. In our study, we transplanted CB-derived hHSCs into neonatal NOG mice by hepatic injection. Neonatal mice are thought to be better recipients for CB-derived hHSCs transplantation with regard to both engraftment and immune reconstitution as compared to their adult counterpart [15,16]. Indeed, like adult NOG mice transplanted with hHSCs, hHSCs in our NOG-hCD34 mice differentiated into mature T lymphocytes, B lymphocytes, monocytes, and DCs (Table 1

and not shown). High level of HIV-1 viremia (Fig. 1A) and HIV-1 antigen-expressing cells (Fig. 1B) were detected in these mice when they were infected with HIV-1_{JR-CSF}. The extent of human immune cell reconstitution, the duration in which the human cells were maintained, and the level of HIV-1 replication were comparable to those observed in the hHSCs-transplanted adult NOG mice [12,13] and hHSCs-transplanted Rag2$^{-/-}\gamma_c^{-/-}$ mice [16]. Class-switching of antibodies and the production of HIV-1-specific IgG were also observed in NOG-hCD34 mice (Fig. 2), as were observed in hHSCs-transplanted adult NOG mice [12]. Moreover, effector/memory CD8$^+$ T lymphocytes proliferated in response to HIV-1 infection (Fig. 1E–L). These data indicate that NOG-hCD34 mice have strong potential as an animal model for HIV-1 infection.

In both humans and mice, T lymphocyte precursors are selected in the thymus by thymic epithelial cells and DCs expressing major histocompatibility complexes (MHCs). Previous studies [26] and our findings shown in Table 1 strongly indicate that the human T lymphocytes are selected and maturated in the murine thymus as normal T lymphocytes need to recognize MHC molecules presented in the thymus to survive [27]. However, it is still uncertain how human T lymphocytes are selected in the recipient murine thymus by murine MHC molecules. It has been shown that mature T lymphocytes can develop from CB-derived mononuclear cell cultures with supplementation of stem cell factor and interleukin-7 but without thymic feeder cells *in vitro* [28], suggesting that development of human T lymphocytes in humanized mice may be independent of murine MHC molecules. On the other hand, others asserted that murine thymus can support human T lymphocyte differentiation via murine MHCs [29,30]. Although it is unclear whether human T lymphocytes *de novo* generated in hHSCs-xenotransplanted humanized mice are selected by human or murine MHCs, it has been reported that T lymphocytes capable of eliciting immune responses can be produced within humanized mice [14,16,23]. For instance, two reports showed that human CD8$^+$ T lymphocytes in the humanized mice infected with Epstein–Barr virus (EBV) massively proliferated, and that the CD8$^+$ T lymphocytes were reactivated *in vitro* by EBV antigens presented on human MHCs to some extent [16,31]. We have also observed the activation and the proliferation of human CD8$^+$ T lymphocytes in EBV-infected NOG-hCD34 mice (our unpublished observation). Although whether these CD8$^+$ T lymphocytes can elicit human MHC-restricted EBV-specific cytotoxic activity is still under investigation, these findings suggest that human CD8$^+$ T lymphocytes differentiated *de novo* in humanized mice may be selected and primed, at least partly, through human MHCs.

CD8$^+$ T lymphocytes can recognize viral peptides bound to MHC class I molecules and induce cytotoxicity against cells bearing the peptide/MHC class I complex, thus eliminating infected cells [32]. It is thought that CD8$^+$ T lymphocyte-mediated immune surveillance plays an important role in fighting against HIV-1 infection [33]. However, naïve CD8$^+$ T lymphocytes are not able to induce cytotoxicity and only become capable of cell killing after priming by antigen presenting cells (APCs) [34]. The priming of CD8$^+$ T lymphocytes requires complex interactions that include the ligation with both antigen peptide-loaded MHC class I and co-stimulatory molecules on APCs [34]. Successful priming of CD8$^+$ T lymphocytes lead to activation and proliferation of CD8$^+$ T lymphocytes, as well as down-regulation of surface CD45RA molecules [34,35]. The proliferation of CD8$^+$ T lymphocytes lacking CD45RA expression (effector/memory CD8$^+$ T lymphocytes) in HIV-1-infected humanized mice suggests that *de novo* generated leukocytes may be able to initiate and maintain HIV-1-specific CD8$^+$ T lymphocyte responses. Although the proliferation of effector/memory CD8$^+$ T lymphocytes was not associated with the reduction in plasma viral load, it is encouraging to know that such a CD8$^+$ T lymphocyte-mediated response against HIV-1 can be produced in hHSCs-transplanted NOG mice. As far as we know, the proliferation of effector/memory CD8$^+$ T lymphocytes in HIV-1 infection has not been reported in hHSCs-transplanted adult NOG mice [12,13], which may offer a broader application for NOG mice that receive neonatal transplantation. The generation of HIV-1-specific adaptive immune responses makes the present NOG-hCD34 mice system a possible candidate for HIV-1 vaccine evaluation.

Being able to allow HIV-1 replication makes hHSCs-transplanted NOG mice a good candidate for the evaluation of anti-HIV-1 drugs. However, it is not known whether hHSCs-transplanted NOG mice provided researchers with ideal system to study the interaction between human leukocytes and HIV-1. Both viral distraction of CD4$^+$ T lymphocytes and dysregulation of lymphocyte homeostasis are thought to contribute to immune deficiency caused by HIV-1 [36–38]. Therefore, it is important to study the effect of HIV-1 on different subsets of lymphocytes using NOG-hCD34 mice. We found that significant amount of both memory and naïve T lymphocytes were produced in NOG-hCD34 mice (data not shown). In addition, we also found that CCR5-tropic HIV-1 infection caused significant depletion of the memory but not the naïve subset of CD4$^+$ T lymphocytes in the periphery, which resulted in the reduction in overall CD4$^+$ T lymphocytes (Fig. 1C and D) (Nie et al., unpublished data). Furthermore, we found that CD4$^+$ T lymphocytes bearing CCR5 were severely reduced in the spleen of HIV-1-infected mice (Nie et al., unpublished data). These suggest that NOG-hCD34 mice can be used to study the dysregulation of CD4$^+$ T lymphocyte homeostasis after HIV-1 infection.

The emergence of severely immunodeficient mice, such as NOG mice and Rag2$^{-/-}\gamma_c^{-/-}$ mice, which can produce human T lymphocytes upon hHSCs transplantation, has made more sophisticated *in vivo* analyses on HIV-1 infection possible. However, the potential of these models to simulate HIV-1 infection and anti-HIV-1 immune response in human is to be explored in detail. Future investigations should include more thorough analyses on *de novo* reconstituted human immune system and how it is altered by HIV-1 infection, so that we can fully utilize this valuable tool.

Acknowledgements

We would like to thank Hiroko Kitayama (Institute for Virus Research, Kyoto University), Hisanori Fujino, Hidefumi Hiramatsu, Toshio Heike, and Tatsutoshi Nakahata (Graduate School of Medicine, Kyoto University) for helping our study. We also would like to express our appreciation for Ms. Kotubu Misawa's dedicated support. This work was supported by Grant-in-Aid for Scientific Research on Priority Areas from the Ministry of Education, Culture, Sports, Sciences, and Technology of Japan, and a Health and Labor Science Research Grant (Research on Publicly Essential Drugs and Medical Devices) from the Ministry of Health, Labor and Welfare of Japan and Japan Human Science Foundation. K.S. was supported by Research Fellowships of the Japan Society for the Promotion of Science for Young Scientists. Y.K. was supported by a grant from the Naito Foundation.

Conflict of interest statement

The authors state that they have no conflict of interest.

References

[1] Fauci AS. The human immunodeficiency virus: infectivity and mechanisms of pathogenesis. Science 1988;239(4840):617–22.
[2] Jamieson BD, Zack JA. Murine models for HIV disease. AIDS 1999;13(Suppl. A):S5–11.
[3] van Maanen M, Sutton RE. Rodent models for HIV-1 infection and disease. Curr HIV Res 2003;1(1):121–30.

[4] McCune J, Kaneshima H, Krowka J, Namikawa R, Outzen H, Peault B, et al. The SCID-hu mouse: a small animal model for HIV infection and pathogenesis. Annu Rev Immunol 1991;9:399–429.
[5] Namikawa R, Kaneshima H, Lieberman M, Weissman IL, McCune JM. Infection of the SCID-hu mouse by HIV-1. Science 1988;242(4886):1684–6.
[6] Kaneshima H, Shih CC, Namikawa R, Rabin L, Outzen H, Machado SG, et al. Human immunodeficiency virus infection of human lymph nodes in the SCID-hu mouse. Proc Natl Acad Sci USA 1991;88(10):4523–7.
[7] Mosier DE, Gulizia RJ, Baird SM, Wilson DB, Spector DH, Spector SA. Human immunodeficiency virus infection of human-PBL-SCID mice. Science 1991;251(4995):791–4.
[8] Jenkins M, Hanley MB, Moreno MB, Wieder E, McCune JM. Human immunodeficiency virus-1 infection interrupts thymopoiesis and multilineage hematopoiesis *in vivo*. Blood 1998;91(8):2672–8.
[9] Berkowitz RD, Alexander S, Bare C, Linquist-Stepps V, Bogan M, Moreno ME, et al. CCR5- and CXCR4-utilizing strains of human immunodeficiency virus type 1 exhibit differential tropism and pathogenesis *in vivo*. J Virol 1998;72(12):10108–17.
[10] Fais S, Lapenta C, Santini SM, Spada M, Parlato S, Logozzi M, et al. Human immunodeficiency virus type 1 strains R5 and X4 induce different pathogenic effects in hu-PBL-SCID mice, depending on the state of activation/differentiation of human target cells at the time of primary infection. J Virol 1999;73(8):6453–9.
[11] Ito M, Hiramatsu H, Kobayashi K, Suzue K, Kawahata M, Hioki K, et al. NOD/SCID/γ_c^{null} mouse: an excellent recipient mouse model for engraftment of human cells. Blood 2002;100(9):3175–82.
[12] Watanabe S, Terashima K, Ohta S, Horibata S, Yajima M, Shiozawa Y, et al. hematopoietic stem cell-engrafted NOD/SCID/IL2Rγ^{null} mice develop human lymphoid system and induce long-lasting HIV-1 infection with specific humoral immune responses. Blood 2007;109(1):212–8.
[13] Watanabe S, Ohta S, Yajima M, Terashima K, Ito M, Mugishima H, et al. Humanized NOD/SCID/IL2Rγ^{null} mice transplanted with hematopoietic stem cells under nonmyeloablative conditions show prolonged life spans and allow detailed analysis of human immunodeficiency virus type 1 pathogenesis. J Virol 2007;81(23):13259–64.
[14] Hiramatsu H, Nishikomori R, Heike T, Ito M, Kobayashi K, Katamura K, et al. Complete reconstitution of human lymphocytes from cord blood CD34$^+$ cells using the NOD/SCID/γ_c^{null} mice model. Blood 2003;102(3):873–80.
[15] Ishikawa F, Yasukawa M, Lyons B, Yoshida S, Miyamoto T, Yoshimoto G, et al. Development of functional human blood and immune systems in NOD/SCID/IL2 receptor γ chain^{null} mice. Blood 2005;106(5):1565–73.
[16] Traggiai E, Chicha L, Mazzucchelli L, Bronz L, Piffaretti JC, Lanzavecchia A, et al. Development of a human adaptive immune system in cord blood cell-transplanted mice. Science 2004;304(5667):104–7.
[17] Koyanagi Y, Miles S, Mitsuyasu RT, Merrill JE, Vinters HV, Chen IS. Dual infection of the central nervous system by AIDS viruses with distinct cellular tropisms. Science 1987;236(4803):819–22.
[18] Koyanagi Y, Tanaka Y, Kira J, Ito M, Hioki K, Misawa N, et al. Primary human immunodeficiency virus type 1 viremia and central nervous system invasion in a novel hu-PBL-immunodeficient mouse strain. J Virol 1997;71(3):2417–24.
[19] Sato K, Aoki J, Misawa N, Daikoku E, Sano K, Tanaka Y, et al. Modulation of human immunodeficiency virus type 1 infectivity through incorporation of tetraspanin proteins. J Virol 2008;82(2):1021–33.
[20] Okuma K, Tanaka R, Ogura T, Ito M, Kumakura S, Yanaka M, et al. Interleukin-4-transgenic hu-PBL-SCID mice: a model for the screening of antiviral drugs and immunotherapeutic agents against X4 HIV-1 viruses. J Infect Dis 2008;197(1):134–41.
[21] Dejucq N, Simmons G, Clapham PR. Expanded tropism of primary human immunodeficiency virus type 1 R5 strains to CD4$^+$ T-cell lines determined by the capacity to exploit low concentrations of CCR5. J Virol 1999;73(9):7842–7.
[22] Hockett RD, Kilby JM, Derdeyn CA, Saag MS, Sillers M, Squires K, et al. Constant mean viral copy number per infected cell in tissues regardless of high, low, or undetectable plasma HIV RNA. J Exp Med 1999;189(10):1545–54.
[23] Legrand N, Weijer K, Spits H. Experimental models to study development and function of the human immune system *in vivo*. J Immunol 2006;176(4):2053–8.
[24] Kerre TC, De Smet G, De Smedt M, Zippelius A, Pittet MJ, Langerak AW, et al. Adapted NOD/SCID model supports development of phenotypically and functionally mature T cells from human umbilical cord blood CD34$^+$ cells. Blood 2002;99(5):1620–6.
[25] Gimeno R, Weijer K, Voordouw A, Uittenbogaart CH, Legrand N, Alves NL, et al. Monitoring the effect of gene silencing by RNA interference in human CD34$^+$ cells injected into newborn RAG2$^{-/-}\gamma_c^{-/-}$ mice: functional inactivation of p53 in developing T cells. Blood 2004;104(13):3886–93.
[26] Macchiarini F, Manz MG, Palucka AK, Shultz LD. Humanized mice: are we there yet? J Exp Med 2005;202(10):1307–11.
[27] Liu YJ. A unified theory of central tolerance in the thymus. Trends Immunol 2006;27(5):215–21.
[28] Sanchez M, Alfani E, Visconti G, Passarelli AM, Migliaccio AR, Migliaccio G. Thymus-independent T-cell differentiation *in vitro*. Br J Haematol 1998;103(4):1198–205.
[29] Robin C, Bennaceur-Griscelli A, Louache F, Vainchenker W, Coulombel L. Identification of human T-lymphoid progenitor cells in CD34$^+$ CD38^{low} and CD34$^+$ CD38$^+$ subsets of human cord blood and bone marrow cells using NOD-SCID fetal thymus organ cultures. Br J Haematol 1999;104(4):809–19.
[30] Weekx SF, Snoeck HW, Offner F, De Smedt M, Van Bockstaele DR, Nijs G, et al. Generation of T cells from adult human hematopoietic stem cells and progenitors in a fetal thymic organ culture system: stimulation by tumor necrosis factor-α. Blood 2000;95(9):2806–12.
[31] Yajima M, Imadome KI, Nakagawa A, Watanabe S, Terashima K, Nakamura H, et al. A new humanized mouse model of Epstein-Barr virus infection that reproduces persistent infection, lymphoproliferative disorder, and cell-mediated and humoral immune responses. J Infect Dis 2008;198(5):673–82.
[32] Hislop AD, Taylor GS, Sauce D, Rickinson AB. Cellular responses to viral infection in humans: lessons from Epstein-Barr virus. Annu Rev Immunol 2007;25:587–617.
[33] Vasan S, Schlesinger SJ, Arrode G. T cell immune responses to HIV-1. Front Biosci 2007;12:2330–43.
[34] Steinman RM. The dendritic cell system and its role in immunogenicity. Annu Rev Immunol 1991;9:271–96.
[35] Clement LT. Isoforms of the CD45 common leukocyte antigen family: markers for human T-cell differentiation. J Clin Immunol 1992;12(1):1–10.
[36] Centlivre M, Sala M, Wain-Hobson S, Berkhout B. In HIV-1 pathogenesis the die is cast during primary infection. AIDS 2007;21(1):1–11.
[37] Brenchley JM, Schacker TW, Ruff LE, Price DA, Taylor JH, Beilman GJ, et al. CD4$^+$ T cell depletion during all stages of HIV disease occurs predominantly in the gastrointestinal tract. J Exp Med 2004;200(6):749–59.
[38] Okoye A, Meier-Schellersheim M, Brenchley JM, Hagen SI, Walker JM, Rohankhedkar M, et al. Progressive CD4$^+$ central memory T cell decline results in CD4$^+$ effector memory insufficiency and overt disease in chronic SIV infection. J Exp Med 2007;204(9):2171–85.

JOURNAL OF VIROLOGY, Sept. 2010, p. 9546–9556 Vol. 84, No. 18
0022-538X/10/$12.00 doi:10.1128/JVI.00823-10

Remarkable Lethal G-to-A Mutations in *vif*-Proficient HIV-1 Provirus by Individual APOBEC3 Proteins in Humanized Mice[▽]†

Kei Sato,[1]‡ Taisuke Izumi,[2,3] Naoko Misawa,[1] Tomoko Kobayashi,[1] Yoshiki Yamashita,[4] Masahide Ohmichi,[4] Mamoru Ito,[5] Akifumi Takaori-Kondo,[2] and Yoshio Koyanagi[1]*

Laboratory of Viral Pathogenesis, Institute for Virus Research, Kyoto University, 53 Shogoinkawara-cho, Sakyo-ku, Kyoto, Kyoto 606-8507, Japan[1]; Department of Hematology and Oncology, Graduate School of Medicine, Kyoto University, 54 Shogoinkawara-cho, Sakyo-ku, Kyoto, Kyoto 606-8507, Japan[2]; Japanese Foundation for AIDS Prevention, 1-3-12 Misaki-cho, Chiyoda-ku, Tokyo 101-0061, Japan[3]; Department of Gynecology, Osaka Medical College, 2-7 Daigaku-machi, Takatsuki, Osaka 569-8686, Japan[4]; and Central Institute for Experimental Animals, 1430 Nogawa, Miyamae-ku, Kawasaki, Kanagawa 216-0001, Japan[5]

Received 18 April 2010/Accepted 28 June 2010

Genomic hypermutation of RNA viruses, including human immunodeficiency virus type 1 (HIV-1), can be provoked by intrinsic and extrinsic pressures, which lead to the inhibition of viral replication and/or the progression of viral diversity. Human APOBEC3G was identified as an HIV-1 restriction factor, which edits nascent HIV-1 DNA by inducing G-to-A hypermutations and debilitates the infectivity of *vif*-deficient HIV-1. On the other hand, HIV-1 Vif protein has the robust potential to degrade APOBEC3G protein. Although subsequent investigations have revealed that lines of APOBEC3 family proteins have the capacity to mutate HIV-1 DNA, it remains unclear whether these endogenous APOBEC3s, including APOBEC3G, contribute to mutations of *vif*-proficient HIV-1 provirus *in vivo* and, if so, what is the significance of these mutations. In this study, we use a human hematopoietic stem cell-transplanted humanized mouse (NOG-hCD34 mouse) model and demonstrate the predominant accumulation of G-to-A mutations in *vif*-proficient HIV-1 provirus displaying characteristics of APOBEC3-mediated mutagenesis. Notably, the APOBEC3-associated G-to-A mutation of HIV-1 DNA that leads to the termination of translation was significantly observed. We further provide a novel insight suggesting that HIV-1 G-to-A hypermutation is independently induced by individual APOBEC3 proteins. In contrast to the prominent mutation in intracellular proviral DNA, viral RNA in plasma possessed fewer G-to-A mutations. Taken together, these results provide the evidence indicating that endogenous APOBEC3s are associated with G-to-A mutation of HIV-1 provirus *in vivo*, which can result in the abrogation of HIV-1 infection.

Human apolipoprotein B mRNA-editing enzyme catalytic polypeptide-like 3 (APOBEC3 [A3]) family proteins are potent mutators of a broad spectrum of retroviruses, including human immunodeficiency virus type 1 (HIV-1) (4, 5, 13, 16, 29, 61). A3s are cellular cytidine deaminases that convert C in the viral minus-strand cDNA to U, resulting in the alteration of G to A in the nascent proviral DNA. Several A3 proteins are incorporated into progeny virions and mutate viral cDNA in the invaded cells, which is thought to result in the inhibition of viral replication (4, 5, 13, 16, 29, 46, 61). On the other hand, an HIV-1 accessory protein, viral infectivity factor (Vif), has the ability to counteract the incorporation of certain A3 proteins such as A3G and A3F into progeny virions by degrading these proteins through the proteasome-dependent pathway (31, 45, 47, 50). Lines of *in vitro* investigations have elucidated the mechanisms of G-to-A hypermutation of HIV-1 DNA mediated by A3s and the counteracting ability of Vif against A3s, which have shed light on the relevance of host-retrovirus interaction (4, 5, 21, 59, 60). Nevertheless, the physiological balance between intrinsic A3s and Vif *in vivo* is poorly understood, and the significance of A3-mediated mutagenesis for HIV-1 replication *in vivo* remains unresolved.

In order to investigate the dynamics of human-specific pathogens *in vivo*, we have recently constructed a humanized mouse (NOG-hCD34 mouse) model by xenotransplanting human $CD34^+$ hematopoietic stem cells into an immunodeficient NOD/SCID/IL-2R-γ^{null} (NOG) mouse (15, 34). In the humanized mice, human leukocytes, including human $CD4^+$ T cells, are successfully differentiated *de novo* and are stably and longitudinally maintained for more than 1 year (15, 34). By utilizing the humanized mice, we have established a novel animal model for HIV-1 infection (34). Our humanized mice are capable of supporting persistent replication of CCR5-tropic HIV-1 for more than 7 months and mirror the characteristics of HIV-1 pathogenesis, such as the depletion of memory $CD4^+$ T cells in the periphery and the preferential infection of effector memory T cells (34).

Recently, Ince et al. reported the significance of HIV-1 mutation and its influence on HIV-1 expansion by using a humanized mouse model system (14). In that paper, however, the authors particularly focused on the diversity of the HIV-1 *env* gene, and therefore, the involvement and the significance

* Corresponding author. Mailing address: 53 Shogoinkawara-cho, Sakyo-ku, Kyoto, Kyoto 606-8507, Japan. Phone: 81-75-751-4811. Fax: 81-75-751-4812. E-mail: ykoyanag@virus.kyoto-u.ac.jp.
‡ Present address: Center for Emerging Virus Research, Kyoto University, Kyoto, Japan.
† Supplemental material for this article may be found at http://jvi.asm.org/.
▽ Published ahead of print on 7 July 2010.

of A3-associated mutagenesis in HIV-1 expansion *in vivo* remain unclear.

In this study, by using the humanized mouse (NOG-hCD34 mouse) model, we show that G-to-A mutation of *vif*-proficient HIV-1 provirus exhibiting the characteristics of A3-mediated mutagenesis occurs *in vivo*. We also provide a novel insight indicating that intrinsic A3-mediated G-to-A mutation is independently caused by endogenous A3 protein. Furthermore, in contrast to the prominent accumulation of G-to-A mutation in provirus, we observed few mutations in virion-associated RNA in plasma. Based on our findings, we discuss the possibility that endogenous A3s have a significant influence on HIV-1 infection *in vivo*.

MATERIALS AND METHODS

Ethics statement. All protocols involving human subjects were reviewed and approved by the Kyoto University institutional review board. Informed written consent from the human subjects was obtained in this study.

Humanized mice. NOG mice (15) were obtained from the Central Institute for Experimental Animals (Kanagawa, Japan). The mice were maintained under specific-pathogen-free conditions and were handled in accordance with the Regulation on Animal Experimentation at Kyoto University. Human $CD34^+$ hematopoietic stem cells were isolated from human cord blood as described previously (34). Fresh human cord blood was obtained with parental written informed consent from healthy full-term newborns. To construct the humanized mice (NOG-hCD34 mice), the obtained human $CD34^+$ cells (5×10^4 to 12×10^4 cells) were intrahepatically injected into newborn NOG mice aged 0 to 2 days after X-irradiation (10 cGy per mouse) in an RX-650 X-ray cabinet system (Faxitron X-ray Corporation).

HIV-1 infection. Virus solutions of wild-type (WT) HIV-$1_{JR\text{-}CSF}$ (22) and *vif*-deficient HIV-$1_{JR\text{-}CSF}$ (19) were prepared and titrated as previously described (34). Virus solutions containing 10 ng of p24 antigen (equivalent to 10^5 50% tissue culture infective doses [$TCID_{50}$] of HIV-$1_{JR\text{-}CSF}$) were intraperitoneally inoculated into 12- to 13-week-old NOG-hCD34 mice. RPMI 1640 was used as the mock infection. The amount of HIV-1 RNA in plasma, the amount of HIV-1 DNA in splenic human mononuclear cells (MNCs), and the proportion of $p24^+$ cells in splenic human MNCs were analyzed as described previously (34). The proportions of whole $CD4^+$ cells, naïve $CD4^+$ ($CD4^+$ CD45 RO^-) cells, and memory $CD4^+$ ($CD4^+$ CD45 RO^+) cells in human leukocytes ($CD45^+$ cells) of NOG-hCD34 peripheral blood mononuclear cells (PBMCs) were routinely analyzed by flow cytometry as previously described (34). For *in vitro* HIV-1 replication assays, human MNCs were isolated from the spleen of NOG-hCD34 mice and human T cells were expanded by using Dynabeads Human T-Activator CD3/CD28 for cell expansion and activation Invitrogen). The activated human T cells were infected with WT and *vif*-deficient HIV-$1_{JR\text{-}CSF}$ (50 ng of p24) for 2 h at 37°C and were then washed three times. Culture supernatants were routinely harvested, and the amount of HIV-1 p24 antigen was quantified by enzyme-linked immunosorbent assay (ELISA) using an HIV-1 p24 antigen ELISA kit (ZetroMetrix).

Real-time RT-PCR for *A3* genes. Human PBMCs and human MNCs in the spleen of the humanized mice were isolated as previously described (34). These cells were stained with anti-human CD45-phycoerythrin (PE) (BioLegend), anti-human CD3-allophycocyanin (APC) (BioLegend), and anti-human CD4-fluorescein isothiocyanate (FITC) (eBioscience), and human $CD4^+$ T cells ($CD45^+$ $CD3^+$ $CD4^+$ cells) were isolated by using FACSAria (BD Biosciences). The purity was >95%. Total RNA was extracted from the isolated cells by using the mirVana microRNA isolation kit (Ambion), and cDNA was synthesized from the total RNA by using oligo(dT) and the PrimeScript reverse transcriptase PCR (RT-PCR) kit (TaKaRa). Real-time RT-PCR was set up in 20 μl of SYBR Premix EX *Taq* (TaKaRa) with the obtained cDNA and each primer pair for the target genes and was performed by using the Thermal Cycler Dice real-time system (TaKaRa). The primer sequences used in this study were described in a previous study (52). The level of mRNA expression of the target genes (*A3B*, *A3C*, *A3DE*, *A3F*, and *A3G*) in each sample was normalized to that of the glyceraldehyde-3-phosphate dehydrogenase (GAPDH) gene.

Sequencing analysis. Human MNCs in the spleen of 5 WT HIV-1-infected humanized mice at 15 weeks postinfection (wpi) were isolated, and DNA was extracted from these cells by the urea lysis method as previously described (34). Viral RNA was extracted from the plasma of 5 WT HIV-1-infected mice at 15 wpi by using the QIAamp viral RNA minikit (Qiagen). Reverse transcription was performed by using SuperScript III reverse transcriptase (RT) (Invitrogen) and oligo(dT) (Invitrogen) according to the manufacturer's procedure. The 1,002-bp target sequence in the *pol* region (nucleotides 2620 to 3621) was amplified by conventional PCR (2 min at 95°C; 30 s at 95°C, 1 min at 58°C, and 1 min at 72°C for 40 cycles; 10 min at 72°C) using *PfuUltra* high-fidelity DNA polymerase (Stratagene) and the following primers: forward, 5′-GCG AAT TCG CCA GGA ATG GAT GGC CCA A-3′; reverse, 5′-GCG GAT CCG GCA CCC CTC GTT CTT GCA T-3′. The 579-bp *vif* coding sequence was also amplified as described above, and the following primers were used: forward, 5′-GCG AAT TCG GAC CAG CAA AGC TTC TCT G-3′; reverse, 5′-GCG GAT CCC TAT GGA GCC AGA TCC TAG G-3′. The amplified products were digested with EcoRI and BamHI and were inserted into the EcoRI-BamHI site of pUC19 (TaKaRa). The sequencing PCR was set up in 20 μl of the BigDye Terminator v3.1 cycle sequencing kit (Applied Biosystems) with the obtained plasmid and M13 primers (TaKaRa) and was performed by using the ABI Prism 3100 genetic analyzer (Applied Biosystems). Data were analyzed by DNASIS Pro (Hitachi). Maximum likelihood trees of the 1,002-bp target sequence in the *pol* region (nucleotides 2620 to 3621) of proviral DNA and viral RNA were prepared by using ClustalX (v.2.0.12) and NJplot (v.2.3). Bootstrap values were calculated by using NJplot (v.2.3).

RT-PCR for *vif*. RNA was extracted from splenic human MNCs of 5 WT HIV-1-infected mice and 1 mock-infected mouse at 15 wpi by the urea lysis method as previously described (34). The obtained RNA solution was treated with DNase I (Ambion) according to the manufacturer's protocol, and complete removal of DNA in the solution was confirmed by PCR. Reverse transcription was performed by using High-Capacity cDNA reverse transcription kits (Applied Biosciences). RT-PCR for *vif* was performed by using AmpliTaq Gold (Applied Biosciences) with the following primers: forward, 5′-GGG GTC TGC ATA CAG GAG AA-3′; reverse, 5′-TGG GGC TTG TTC CAT CTA TC-3′.

Cotransfection, TZM-bl assay, and Western blotting. Four kinds of Vif mutants (G87A, T92G, G376A, and C540T for nucleotides) were subcloned into a pDon-AI expression plasmid (TaKaRa). Then, one of these four mutated Vif-expressing plasmids or a WT Vif-expressing plasmid (0.5 μg) was cotransfected with pJR-CSFΔ*vif* (0.5 μg) into HEK293T cells stably expressing hemagglutinin (HA)-tagged A3G (HA-A3G) by using Lipofectamine 2000 (Invitrogen) as previously described (44). Four hours after transfection, culture medium was replaced with fresh medium. The culture supernatant was harvested, centrifuged, and then filtrated with a 0.45-μm filter (Millipore) to produce virus solutions at 48 h posttransfection. Titration of the released HIV-1 was performed by using TZM-bl cells as previously described (44). For Western blot analysis of the released virion, 1 ml of virus solution was ultracentrifuged at 30,000 rpm for 1 h at 4°C by using TL-100 (Beckman), and the following procedure was performed as previously described (43, 44). Anti-HA antibody (3F10; Roche) and anti-p24 antiserum (ViroStat) were used for the detection. HEK293T cells stably expressing HA-A3G were established by transfecting pcDNA3.1-HA-A3G and were maintained in Dulbecco's modified Eagle medium (Sigma) containing 10% fetal calf serum, antibiotics, 1% GlutaMax (Invitrogen), and 500 μg/ml hygromycin (Invitrogen).

Statistical analyses. Data were expressed as averages with standard errors of the means (SEMs). Significant differences ($P < 0.05$) were determined by Student's *t* test (Fig. 1). To determine statistical difference for the independence between the obtained raw values and the stochastically expected value (Fig. 2, 4, and 5), the χ^2 test for independence was applied and a *P* value of <0.05 was considered significant.

Nucleotide sequence accession numbers. The GenBank (http://www.ncbi.nlm.nih.gov/GenBank/index.html) accession numbers for the genes and virus mentioned in the text are as follows: *A3B* (NM_004900), *A3C* (NM_014508), *A3DE* (NM_152426), *A3F* (NM_145298), *A3G* (NM_021822), *GAPDH* (NM_002046), and HIV-$1_{JR\text{-}CSF}$ (M38429).

RESULTS

Vif is crucial for HIV-1 expansion in humanized mice. To embark on determining the relevance between endogenous A3s and HIV-1 hypermutation *in vivo*, we first analyzed the mRNA expression levels of *A3* genes (*A3B*, *A3C*, *A3DE*, *A3F*, and *A3G*) in splenic human $CD4^+$ T cells, which are differentiated in the humanized mice. Six humanized mice, which were respectively reconstituted from 6 separate individual cord blood donors, were used for these analyses with no significant

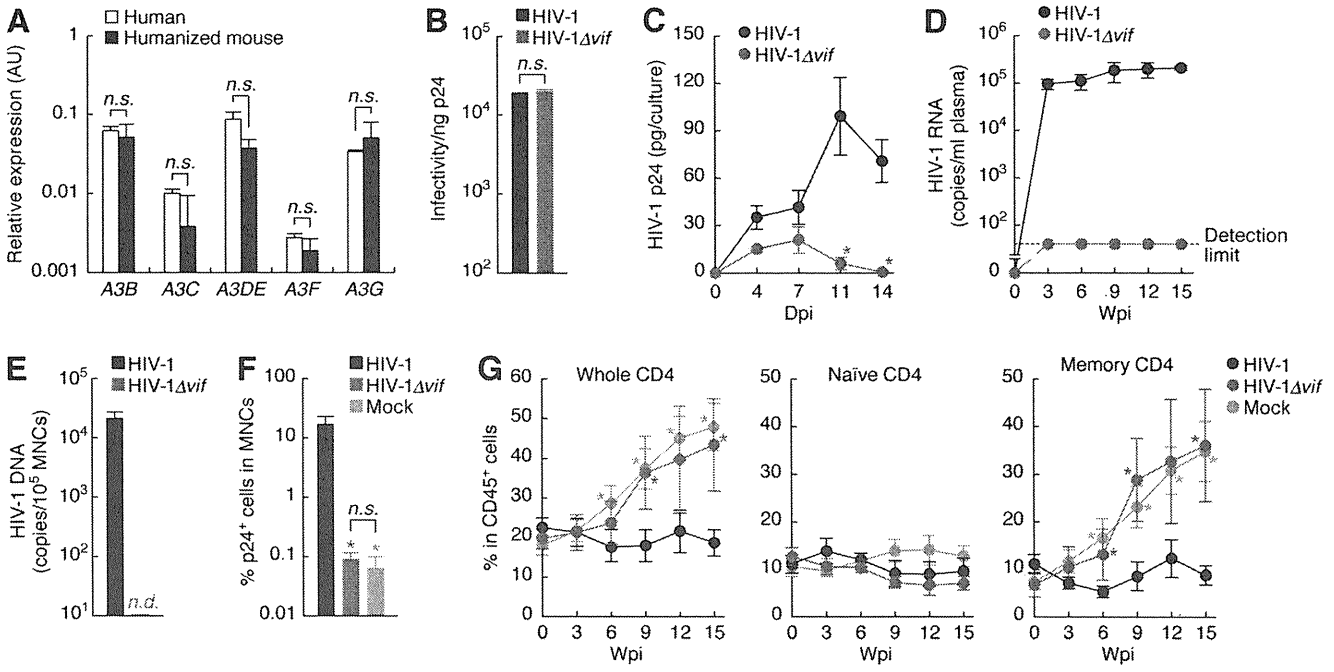

FIG. 1. Relevance of endogenous A3s and Vif in humanized mice. (A) Comparison of the expression levels of *A3* genes in $CD4^+$ T cells from humans and the humanized mice. Human $CD4^+$ T cells in PBMCs of humans ($n = 7$) and those in the spleen of the humanized mice ($n = 6$) were isolated. The expression levels of *A3B*, *A3C*, *A3DE*, *A3F*, and *A3G* were analyzed by real-time RT-PCR and were normalized to *GAPDH*. (B) Infectivities of WT and *vif*-deficient HIV-1. WT and *vif*-deficient $HIV\text{-}1_{JR\text{-}CSF}$ were prepared as described in Materials and Methods and were inoculated into TZM-bl indicator cells. The infectivities of these viruses were quantified as described in Materials and Methods and were normalized to the amount of p24. The assay was performed in triplicate, and a representative result is shown. (C) *In vitro* replication of WT and *vif*-deficient HIV-1. WT and *vif*-deficient $HIV\text{-}1_{JR\text{-}CSF}$ were inoculated into the activated human T cells isolated from the spleen of humanized mice. The culture supernatants were routinely harvested, and the amount of p24 was quantified by ELISA. The assay was performed in triplicate, and a representative result is shown. (D) Longitudinal analysis of HIV-1 replication in humanized mice. WT ($n = 15$) and *vif*-deficient ($n = 6$) $HIV\text{-}1_{JR\text{-}CSF}$ were inoculated into 12- to 13-week-old humanized mice, and the amount of HIV-1 RNA in plasma was routinely analyzed. The horizontal broken line indicates the detection limit of the assay (40 copies/ml). (E and F) The levels of HIV-1 DNA and HIV-1-infected cells in spleen. The copy number of HIV-1 DNA in 10^5 splenic human MNCs of WT ($n = 7$) and *vif*-deficient ($n = 4$) $HIV\text{-}1_{JR\text{-}CSF}$-infected mice (E) and the percentage of HIV-1 p24-positive cells in splenic human MNCs of WT ($n = 6$) and *vif*-deficient ($n = 5$) $HIV\text{-}1_{JR\text{-}CSF}$-infected mice and mock-infected mice ($n = 4$) (F) were determined. (G) Proportion of peripheral $CD4^+$ cells. The percentages of whole $CD4^+$ cells, naïve $CD4^+$ cells, and memory $CD4^+$ cells in human $CD45^+$ leukocytes of WT ($n = 15$) and *vif*-deficient ($n = 6$) $HIV\text{-}1_{JR\text{-}CSF}$-infected mice and mock-infected mice ($n = 14$) were routinely analyzed. Asterisks indicate statistically significant differences from the value of WT HIV-1 ($P < 0.05$ by Student's *t* test). Error bars represent SEMs. AU, arbitrary unit; Dpi, days postinfection; Wpi, weeks postinfection; *n.d.*, not detected; *n.s.*, no statistical significance.

differences observed between each donor and any other (data not shown). We then compared A3 expression levels in these mice to those in human peripheral $CD4^+$ T cells. As shown in Fig. 1A, we found that the relative mRNA levels of *A3* genes in human $CD4^+$ T cells of humanized mice were comparable to those in PBMCs of humans. These results indicate that the effect of endogenous A3s on HIV-1 replication in humanized mice can reflect that in humans.

To assess the importance of Vif for HIV-1 replication *in vivo*, we next prepared a CCR5-tropic HIV-1 molecular clone ($HIV\text{-}1_{JR\text{-}CSF}$) and its *vif*-deficient derivative (HIV-1Δ*vif*) by transfecting pJR-CSF and pJR-CSFΔ*vif* (19) into 293T cells, which did not express any A3 proteins. We found that the infectivity of *vif*-deficient $HIV\text{-}1_{JR\text{-}CSF}$ was comparable to that of WT $HIV\text{-}1_{JR\text{-}CSF}$ (Fig. 1B). On the other hand, as previously found in human PBMC culture (19), HIV-1Δ*vif* did not replicate in the cultured human $CD4^+$ T cells that were isolated from the spleen of humanized mice (Fig. 1C). We then inoculated WT and *vif*-deficient $HIV\text{-}1_{JR\text{-}CSF}$ into the humanized mice. Although WT HIV-1 longitudinally replicated in the infected mice (Fig. 1D to F), we could not detect HIV-1 RNA in the plasma (Fig. 1D), HIV-1 proviral DNA in the spleen (Fig. 1E), or HIV-1-infected cells in the spleen (Fig. 1F) of HIV-1Δ*vif*-infected mice. In addition, WT HIV-1-infected mice showed a significant reduction of human $CD4^+$ cells, especially memory $CD4^+$ cells, whereas the reduction of $CD4^+$ cells was not observed in HIV-1Δ*vif*-infected mice (Fig. 1G). These results indicate that Vif is indispensable for HIV-1 expansion in the humanized mice and that the counteracting ability of Vif against certain A3s is crucial for HIV-1 expansion *in vivo*.

G-to-A mutation predominantly occurs in WT HIV-1-infected humanized mice and exhibits the hallmark of A3-mediated mutagenesis. It has been reported that A3-mediated mutagenesis frequently targets the proximal upstream regions of both the central and 3′ polypurine tracts (51). Therefore, in order to investigate the mutation frequency of HIV-1 *in vivo*, we focused on the *pol* region, which is located upstream of the central polypurine tract. Since HIV-1Δ*vif* did not replicate in humanized mice (Fig. 1D to F), the sequencing analysis was applicable only to WT HIV-1-infected mice. DNA was ex-

TABLE 1. Profiles of 5 WT HIV-1_{JR-CSF}-infected NOG-hCD34 mice used for sequencing analysis

Mouse no.[a]	Transplanted hHSC		HIV-1 RNA[d]	% $CD45^+$ cells in PB[e]		% CD4 cells[f]						No. of sequenced amplicons[g]
						Whole		Naïve		Memory		
	Donor[b]	No.[c]		0 wpi	15 wpi	0 wpi	15 wpi	0 wpi	15 wpi	0 wpi	15 wpi	
1	A	40,000	376,000	51.6	55.8	13.0	28.6	6.2	2.3	6.8	26.3	30
2	A	40,000	26,000	22.0	32.5	25.1	12.8	15.1	3.3	10.0	9.5	43
3	A	40,000	14,600	20.1	35.5	36.1	9.3	22.7	2.1	13.4	7.2	30
4	B	66,000	11,500	7.9	5.0	48.4	29.8	30.4	16.7	18.0	13.1	70
5	B	66,000	322,000	6.1	5.9	48.0	34.2	32.8	9.0	15.2	25.2	80

[a] The mouse numbers correspond with those in Fig. 3A.
[b] NOG-hCD34 mice were reconstituted with one of two human $CD34^+$ hematopoietic stem cell (hHSC) donors, A and B.
[c] The number of transplanted hHSCs per recipient mouse.
[d] The copy number of HIV-1 RNA per ml plasma at 15 weeks postinfection (wpi).
[e] The percentage of human $CD45^+$ leukocytes in peripheral blood (PB).
[f] The percentages of human $CD4^+$ cells (whole CD4), human $CD4^+$ CD45 RO^- cells (naïve CD4), and human $CD4^+$ CD45 RO^+ cells (memory CD4) in peripheral human $CD45^+$ leukocytes.
[g] The numbers of the sequenced amplicons that were derived from both proviral DNA and viral RNA.

tracted from the splenic human MNCs of 5 WT HIV-1-infected mice at 15 wpi (Table 1), and the 1,002-bp RT coding sequence in the *pol* region (nucleotides 2620 to 3621) was amplified by conventional PCR and was cloned. We sequenced 253 amplicons and detected various sequences (Fig. 6A). Within the sequenced 253,506 nucleotides (including 51,359 Gs), we detected a high frequency of G-to-A mutations (56.3% of total mutations) (Fig. 2A; see also Fig. S1 in the supplemental material).

To examine the trend of G-to-A mutation sites, we assessed the type of nucleotides positioned between −5 and +5 from the detected G-to-A mutated sites. We then compared the actual result to the one expected if all of the G-to-A mutations had stochastically occurred (Fig. 2B). Of note, we found that there was a statistically significant preference ($P = 0.0000012$) only on the nucleotide following the detected G-to-A mutation sites and that both A and G were predominant in the position (52.0% of G-to-A mutation sites were GA-to-AA, whereas 45.4% were GG-to-AG). Extensive *in vitro* studies have demonstrated that each A3 protein preferentially targets the Gs, which are located one base prior to purines (i.e., GG and/or GA). Heretofore *in vitro* observations from the available literature (2, 6, 7, 12, 24, 27, 56, 58) are summarized in Table S1 in the supplemental material. For instance, A3G tends to favor GG-to-AG mutagenesis (74 to 88%), whereas A3F and A3B have preferences for GA-to-AA mutagenesis (76 to 91% and 70 to 85%, respectively). In line with these findings, our results strongly suggest that the majority of G-to-A mutation in HIV-1-infected humanized mice is not randomly induced but is caused by endogenous A3 proteins.

A3-mediated G-to-A mutation is significantly associated with the termination of viral protein translation. To investigate the putative outcome of A3-mediated G-to-A mutation for HIV-1 expansion *in vivo*, a total of 221 G-to-A mutation sites, which were detected in A3 contexts (i.e., GG and/or GA), were distinguished between nonsynonymous and synonymous mutations (i.e., changed and unchanged amino acids, respectively). According to the codon usage, we also detected nonsynonymous G-to-A mutations that result in the termination of translation (i.e., conversion to stop codons) and that are associated with the resistance to conventional anti-HIV-1 drugs (20, 33, 40). As shown in Fig. 2C, the frequencies of nonsynonymous, synonymous, and drug resistance-associated mutations in the observed G-to-A mutation sites were comparable to those in the results expected from random G-to-A mutation. However, it was of interest that the frequency of G-to-A mutation, which introduces a stop codon, was significantly higher than the estimated value (Fig. 2C, $P = 0.039$). These findings suggest that A3-mediated mutagenesis is significantly associated with the creation of stop codons, which result in the cessation of viral replication.

Functional Vif is maintained in the infected mice. Vif is known to be able to impair the action of certain A3s, such as A3G and A3F (31, 45, 47, 50). We detected the successful expression of *vif* in the 5 infected mice used for the sequencing analysis (Fig. 3A). Nevertheless, significant G-to-A mutations exhibiting the hallmark of A3-mediated mutagenesis were detected in the infected mice (Fig. 2). Since it was reported previously that some Vif variants, which lost the counteracting ability against A3s, can naturally emerge in patients (49), we suspected that such a defective Vif variant(s) emerged in the infected mice. To address this possibility, we analyzed the sequence of the *vif* coding region and found that some nonsynonymously mutated derivatives (G87A, T92G, G376A, and C540T for nucleotides) were predominant (Fig. 3B; see also Fig. S2 in the supplemental material). To evaluate the counteracting ability of these Vif mutants against A3s, expression plasmids for these Vif derivatives and WT Vif were cotransfected with a *vif*-deficient HIV-1-producing plasmid (pJR-CSFΔ*vif*) into HEK293T cells stably expressing A3G. These Vif mutants (M29I, I31S, G126R, and A137V for amino acids) were expressed at a level comparable to that for WT Vif (data not shown), and the infectivities of released HIV-1 virions from these transfected cells were also comparable (Fig. 3C, bottom). Moreover, we detected the efficient exclusion of A3G from the released virion by these Vif mutants (Fig. 3C, top). Taken together, these results suggest that the counteracting ability of Vif against A3s was maintained in WT HIV-1-infected humanized mice.

G-to-A hypermutation is caused by individual A3 proteins *in vivo*. To further verify the G-to-A mutation observed in HIV-1-infected humanized mice, the obtained data were analyzed

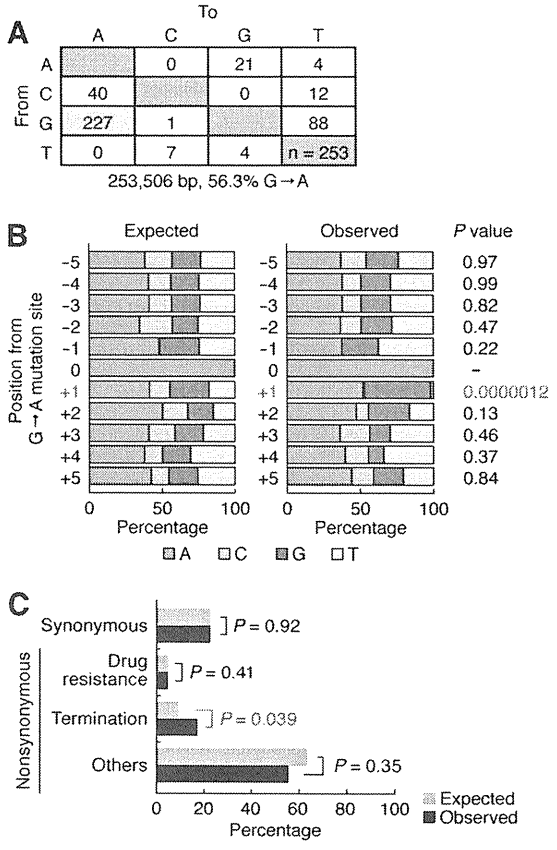

FIG. 2. Preferential G-to-A mutation in HIV-1 provirus *in vivo*. (A) Mutation of HIV-1 provirus in humanized mice. The *pol* region of HIV-1 proviral DNA (1,002 bp, nucleotides 2620 to 3621) was cloned and sequenced, and the mutation matrix is shown. (B) Preference of G-to-A mutation sites. The 227 detected G-to-A mutation sites were classified according to the nucleotides positioned between −5 and +5 from the detected G-to-A mutation sites (position 0). The result obtained (Observed) was compared to the result expected if G-to-A mutation were stochastically induced (Expected). Statistical differences between the obtained and the expected results in each position were determined by the χ^2 test for independence. (C) Classification of the effect of G-to-A mutation on HIV-1 replication. The 221 G-to-A mutations detected in A3 contexts were sorted into synonymous and nonsynonymous mutations. Nonsynonymous mutations were further classified into termination mutations, drug resistance-associated mutations, and missense mutations (Others). The obtained result (Observed) was compared to the result expected if G-to-A mutation were stochastically induced (Expected). Statistical differences between the obtained and the expected results were determined by the χ^2 test for independence.

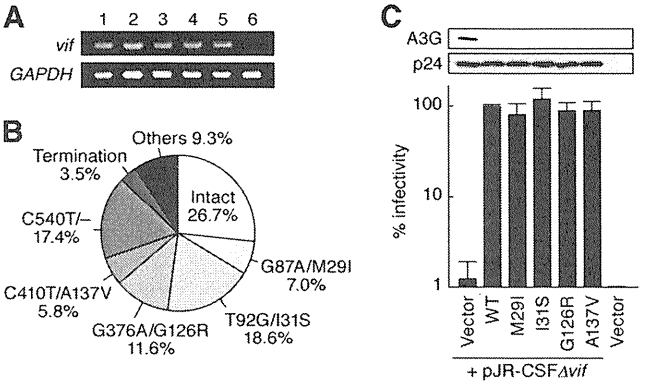

FIG. 3. Functional property of Vif in the infected mice. (A) Expression of *vif* in WT HIV-1-infected mice. The expression of *vif* in the splenic human MNCs of 5 WT HIV-1-infected mice used for sequencing analysis (lanes 1 to 5) and that of a mock-infected mouse (lane 6) were analyzed by RT-PCR. *GAPDH* was used as the positive control of the assay. The mouse numbers correspond with those in Table 1. (B) Diversity of *vif* coding sequences in the infected mice. The coding sequences of *vif* (579 nucleotides, nucleotides 5053 to 5631) were cloned and sequenced, and the distribution of the predominant sequences is shown as the percentage of all sequences (86 amplicons). Nucleotide substitutions (left) and amino acid substitutions (right) are represented. Note that C540T is a synonymous substitution. (C) Evaluation of the ability of mutated Vif to counteract A3G. Four kinds of nonsynonymously mutated (M29I, I31S, G126R, and A137V) Vif-expressing plasmids, WT Vif-expressing plasmid, and the parental plasmid (Vector) were cotransfected with a *vif*-deficient HIV-1-producing plasmid (pJR-CSFΔ*vif*) into HA-A3G-expressing HEK293T cells. The infectivity of HIV-1 virions released from cotransfected cells is shown as the percentage of that from WT Vif-cotransfected cells (bottom). The amount of released HIV-1 virions (p24) and that of A3G in the released virions were analyzed by Western blotting (top). The assay was performed in triplicate, and a representative result is shown. Error bars represent SEMs.

for individual amplicons. We found that 102 of 253 individual amplicons (41.5%) contained mutations and that 9 amplicons possessed more than 10 mutations (Fig. 4A). As summarized in Table 2, 8 out of the 9 hypermutated amplicons predominantly harbored G-to-A substitutions. In addition, 20.3% of the analyzed amplicons (52/253) contained multiple mutations, and 9.2% (23/253) possessed multiple G-to-A mutations (Fig. 4B). We then sorted the 23 amplicons which possessed multiple G-to-A mutations, based on the nucleotide following each mutated site. Of note, we found that either GG-to-AG (9/23) or GA-to-AA (7/23) mutations were significantly predominant in each amplicon possessing multiple G-to-A mutations (Fig. 4C). Furthermore, the biased mutations in the context of GG to AG or GA to AA were abundantly detected in the highly mutated amplicons (Fig. 4D and Table 2). As summarized in Table S1 in the supplemental material, the target preferences of A3G, A3F, and A3B are mostly monistic (GG to AG, GA to AA, and GA to AA, respectively), whereas those of A3C and A3DE are dualistic (GG to AG plus GA to AA and GA to AA plus GT to AT, respectively). Therefore, our findings suggest that G-to-A hypermutation within an amplicon is independently induced by individual A3 proteins, including A3G, A3F, or A3B.

A3-mediated G-to-A mutation is less strongly associated with viral RNA diversity. Since it has been reported elsewhere that viral RNA is less frequently mutated than is proviral DNA in a cell culture experiment (41), we further assessed the mutation level of viral RNA in WT HIV-1-infected mice. Viral RNA was extracted from the plasma of 5 infected mice at 15 wpi, and the 253 amplicons of the 1,002-bp RT coding sequence (nucleotides 2620 to 3621) were analyzed. As found in proviral DNA, a high frequency of G-to-A mutation was also detected in viral RNA (69.6% of total mutations) (Fig. 5A). However, it was notable that there were fewer multiply mutated amplicons in viral RNA, and the number of multiply mutated amplicons from viral RNA was significantly lower than that from proviral DNA (Fig. 5B and C and 6B). Among the 82 amplicons that harbored one G-to-A mutation (Fig.

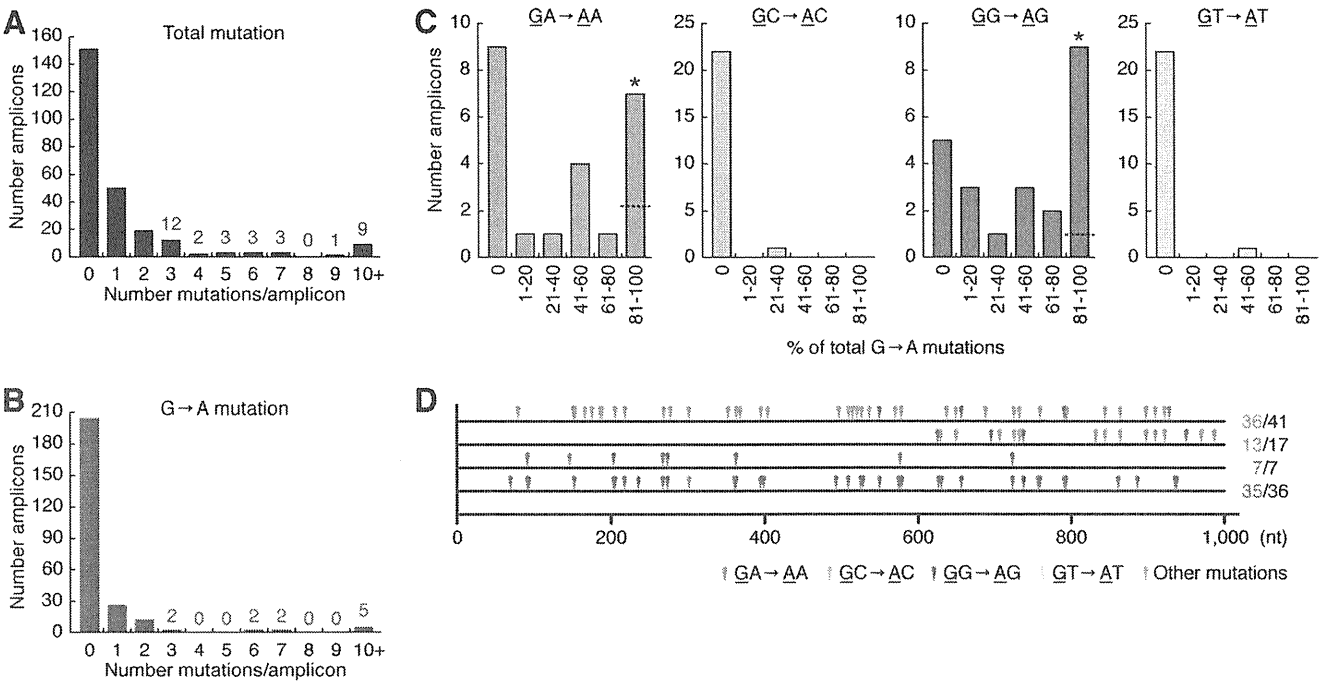

FIG. 4. Biased G-to-A mutation in HIV-1 provirus *in vivo*. (A and B) The extent of mutation in each amplicon of proviral DNA. The number of whole mutations (A) and that of G-to-A mutations (B) within each amplicon (n = 253) are shown. (C and D) The accumulation of either GA-to-AA or GG-to-AG hypermutations within an amplicon. (C) The 23 amplicons that possessed more than 2 G-to-A mutations were sorted by the respective nucleotide next to the detected G-to-A site. The percentage of the type of nucleotides following G-to-A sites in whole G-to-A sites within each amplicon (shown as "% of total G→A mutations" on x axis) was calculated and was further classified into 6 grades (0, 1 to 20, 21 to 40, 41 to 60, 61 to 80, and 81 to 100%). Horizontal broken lines in the graphs of GA→AA and GG→AG (only in 81 to 100%) represent the values expected if G-to-A mutations are stochastically induced. Asterisks indicate statistically significant differences ($P < 0.05$ by χ^2 test for independence) between the obtained and the expected values. (D) Representatives of the amplicons harboring biased G-to-A hypermutations. The sequences of 2 GA-to-AA-biased (top) and 2 GG-to-AG-biased (bottom) amplicons are illustrated. The numbers of GA-to-AA sites (top), GG-to-AG sites (bottom), and total G-to-A mutation sites within the sequenced *pol* region (1,002 nucleotides) are presented at the right of each sequence. Note that GC-to-AC and GT-to-AT mutations were not detected in the 4 amplicons.

5C), 73 out of the 82 amplicons possessed the same substitution (G3335A) (see Fig. S3 in the supplemental material). Since it has been reported previously that there are some hot spots, which are preferentially targeted by A3-mediated mutagenesis (25, 46), the G positioned at 3335 may be one of them. Moreover, a total of 74 G-to-A mutations of viral RNA, which were found in A3 contexts (i.e., GG and/or GA), were classified by their codon mutation. As shown in Fig. 5D, the majority (73/74) of A3-associated G-to-A mutations were synonymous, and the frequency was significantly higher than both the estimated value and the value from proviral DNA. It was also notable that there were neither drug resistance-associated nor termination mutations (Fig. 5D). Taken together, these findings suggest that intrinsic A3-associated mutagenesis is significantly prevalent in proviral DNA and yet does not affect the diversity of viral RNA in humanized mice.

DISCUSSION

To summarize our findings, we have directly demonstrated that G-to-A mutation of proviral DNA is frequently detected in WT HIV-1 replication under a natural environment mirroring physiological circumstances in humans (Fig. 1 and 2). In addition, the detected G-to-A mutation sites significantly exhibited the characteristics of A3-mediated G-to-A mutation observed *in vitro* (Fig. 2B). It has been shown elsewhere that the hypermutated HIV-1 sequences from infected patients exhibit strong preferences for G-to-A mutation, especially for

TABLE 2. Summary of the 9 hypermutated amplicons[a]

Type of mutation value	Value for amplicon no.								
	1	2	3	4	5	6	7	8	9
No. of total	10	11	13	13	17	18	36	42	42
No. of G to A	7	7	7	0	17	10	36	41	41
G to A, % of total	70	64	54	0	100	56	100	98	98
GA to AA, % of G to A	0	0	88		76	0	3	88	88
GG to AG, % of G to A	100	100	12		24	100	97	12	12

[a] The amplicons possessed more than 10 mutations (shown as "10+" in Fig. 4A).

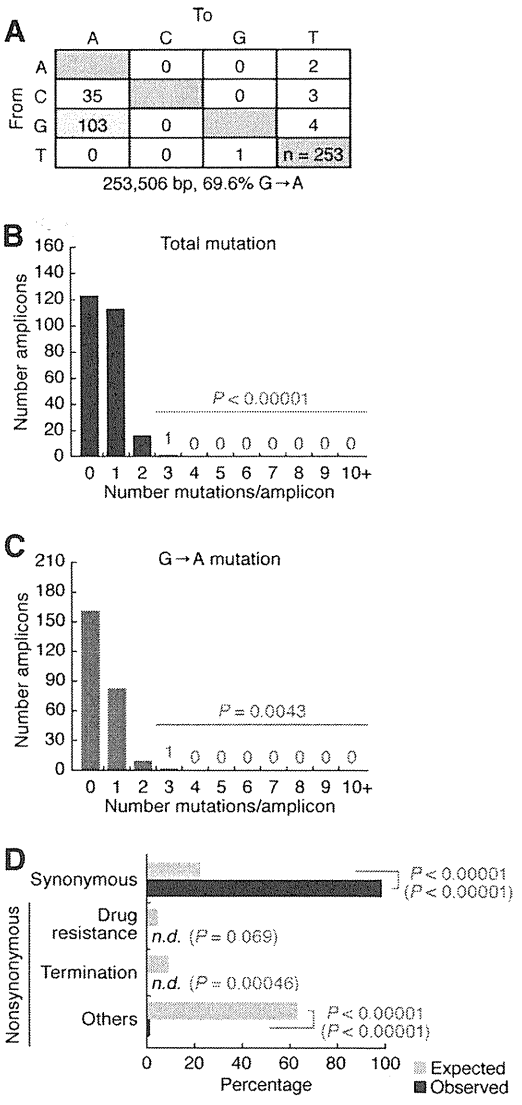

FIG. 5. Few G-to-A mutations in HIV-1 viral RNA *in vivo*. (A) Mutation of HIV-1 RNA in humanized mice. The *pol* region of HIV-1 viral RNA (1,002 bp, nucleotides 2620 to 3621) was cloned and sequenced, and the mutation matrix is shown. (B and C) The extent of mutation in each amplicon of viral RNA. The number of whole mutations (B) and that of G-to-A mutations (C) within each amplicon (n = 253) are shown. Statistical differences between the number of viral RNA amplicons possessing more than 3 mutations and that of proviral DNA were determined by the χ^2 test for independence. (D) Classification of A3-associated G-to-A mutations in viral RNA. The 75 G-to-A mutations detected in A3 contexts were sorted into synonymous and nonsynonymous mutations. Nonsynonymous mutations were further classified into termination mutations, drug resistance-associated mutations, and missense mutations (Others). The result obtained (Observed) was compared to the result expected if G-to-A mutation were stochastically induced (Expected). Statistical differences between the value obtained in viral RNA from the expected results (indicated in red) and the value in proviral DNA (indicated in blue with parentheses) were determined by the χ^2 test for independence. *n.d.*, not detected.

either or both GA to AA and/or GG to AG (9, 11, 17, 20, 23, 26, 36, 39, 53, 57). However, since the original sequences of HIV-1 strains that clinically infected individuals are completely undeterminable, the previous reports of HIV-1 mutation in patients have been mostly based on comparisons to certain HIV-1 laboratory clones (9, 11, 17, 20, 23, 26, 36, 39, 53–55, 57). On the other hand, we were able to track specific mutations from the inoculation with a single HIV-1 molecular clone ($HIV\text{-}1_{JR\text{-}CSF}$) and obtained convincing evidence for the preferential HIV-1 G-to-A mutation in an *in vivo* model. Moreover, most of the G-to-A mutation sites exhibited the characteristics observed in A3-mediated mutation *in vitro*. Although the pronounced G-to-A hypermutation has been detected in the cell culture of activated $CD4^+$ T cells (17, 38), there have been no investigations performed *in vivo*. Taken together, this is the first demonstration suggesting that endogenous A3s have a crucial role as an HIV-1 mutator *in vivo* even under conditions allowing high and prolonged viral replication.

The skewed mutations in the context of GG to AG or GA to AA have been suggested from the observations of clinical specimens (1, 11, 20, 23, 36, 39, 53). However, their extent varies in each individual study and it remains controversial whether A3-mediated G-to-A mutation occurs in either or both contexts in an amplicon. In this study, it was notable that the proviral G-to-A hypermutation in each clone showed predominant skewing to either GG to AG or GA to AA (Fig. 4C and D and Table 2). As described in previous reports, each A3 protein, especially A3G, A3F, or A3B, has its respective major target preference: GG to AG or GA to AA (see Table S1 in the supplemental material). In accordance with our findings, we herein propose a model in which individual A3 family proteins independently participate in G-to-A hypermutation of *vif*-proficient HIV-1 *in vivo*. In fact, it has been reported previously that a small amount of A3G proteins (0.3 to 0.8 molecules per virion) can be incorporated into a WT HIV-1 particle (35). Two enzymological investigations also support the possibility that monomeric A3G protein is capable of tremendous G-to-A hypermutation by jumping, sliding, and/or intersegmentally transferring on single-stranded viral DNA (3, 35). Therefore, our results suggest that an A3 protein, which could circumvent Vif-mediated degradation, may be incidentally causing the biased G-to-A mutation of nascent HIV-1 DNA in the infected cells (Fig. 7, bottom). Although it is still ambiguous which A3(s) is the major determinant(s) for HIV-1 G-to-A hypermutation *in vivo*, our results suggest that certain A3 proteins (e.g., A3G, A3F, and A3B) orchestrally, but independently, contribute to HIV-1 G-to-A hypermutation *in vivo*.

During reverse transcription for the synthesis of nascent minus-strand viral DNA, it is possible for HIV-1 RT to cause nucleotide substitution, including G-to-A substitution (10). However, it would be mostly impossible to distinguish error-prone RT-derived G-to-A substitution from A3-mediated G-to-A mutation. In this regard, we detected some amplicons harboring tremendous G-to-A hypermutation (Fig. 4D and Table 2). Since the error-prone substitution by RT can occur incidentally at a rate of 3×10^{-5} per replication cycle (10, 30), it would be difficult to assume that these G-to-A hypermutated amplicons were derived from error-prone RT-associated substitution. Moreover, we also detected the significant preference of G-to-A mutation in A3-preferred dinucleotide contexts (GG to AG and/or GA to AA) (Fig. 2B). Therefore, these findings suggest that the majority of G-to-A mutations observed in proviral DNA are caused by endogenous A3s.

Since it has been well known that Vif is a potent inhibitor for

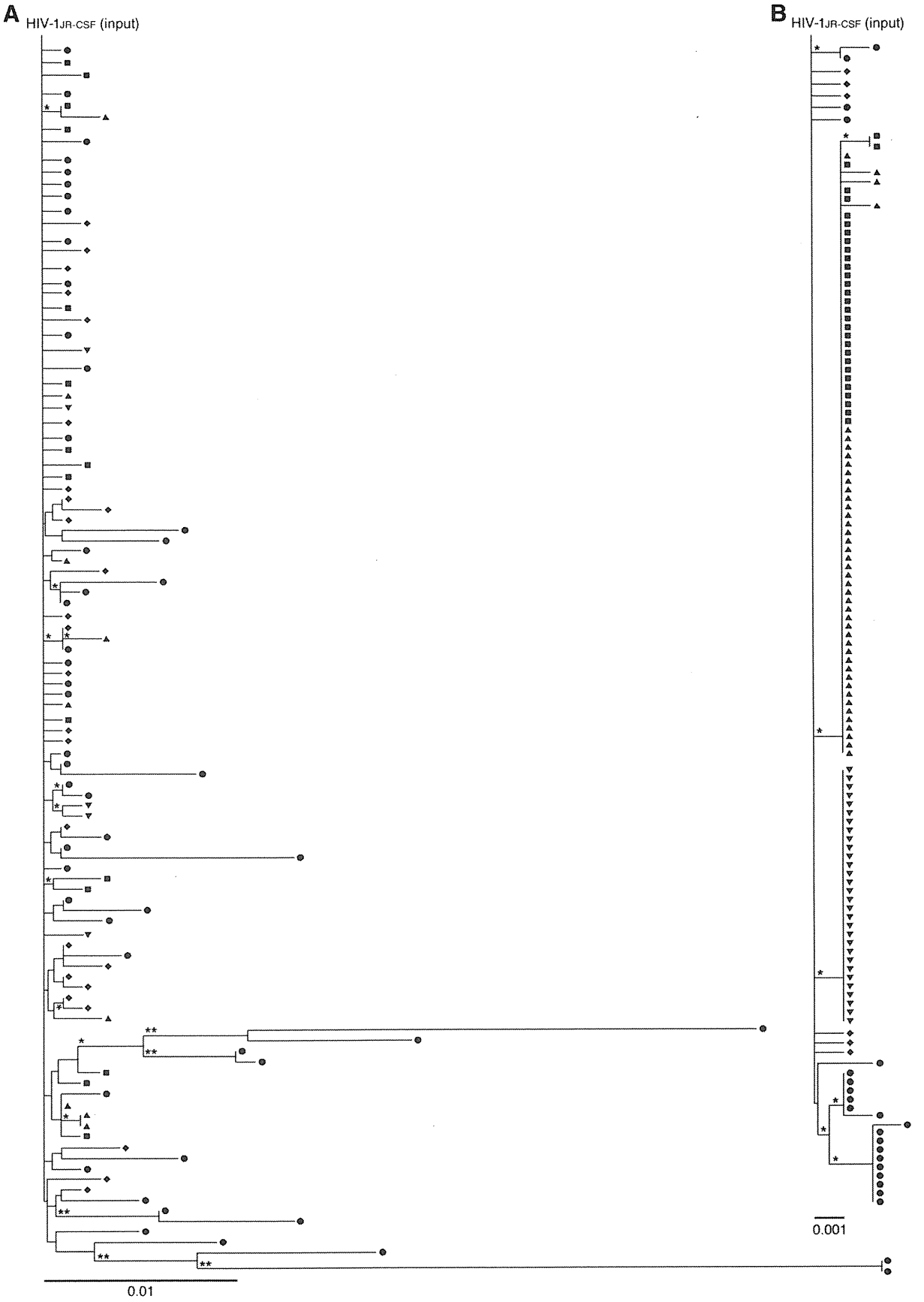

FIG. 6. Phylogeny of proviral DNA and viral RNA in 5 WT HIV-1-infected mice. Maximum likelihood trees of the 1,002-bp *pol* region of HIV-1 proviral DNA (A) and viral RNA (B) are shown. Each symbol represents the result from respective infected mice ($n = 5$). The scale bars indicate the numbers of substitutions per site. Bootstrap values are shown as follows: *, >50%; **, >80%.

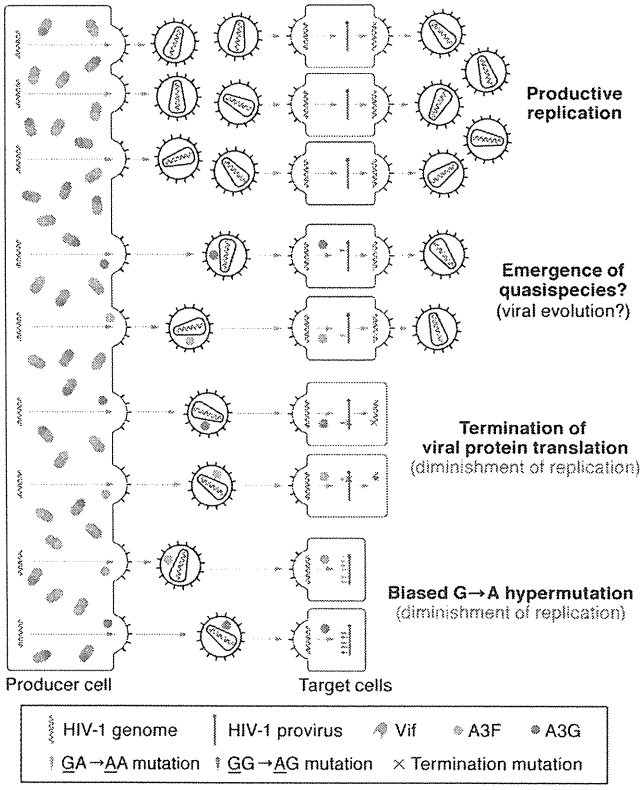

FIG. 7. A possible model for the biased G-to-A mutation in HIV-1 *in vivo*. The dynamics of HIV-1 replication accompanying G-to-A mutagenesis of HIV-1 DNA by A3s are illustrated. (i) The mechanism of action of endogenous A3s. In the presence of Vif, the ability of almost all of the A3 proteins (A3G and A3F) is counteracted by Vif through the proteasome-dependent degradation pathway. Nevertheless, a fraction of A3s that evaded Vif-mediated degradation would be incidentally incorporated into a virion and individually cause the biased G-to-A mutation of HIV-1 reverse-transcribed DNA in the respective infected cells. For instance, A3G induces GG-to-AG-biased mutation, whereas A3F contributes to GA-to-AA-biased mutagenesis (bottom). (ii) The effect of endogenous A3s on HIV-1 expansion *in vivo*. Along with productive replication (top), sublethal G-to-A mutation by endogenous A3s may have been associated with the emergence of HIV-1 quasispecies, leading to viral diversity and evolutionary change (upper middle). In addition, partial G-to-A mutation by intrinsic A3s can significantly evoke the termination mutation (e.g., TGG to TAG), which results in the diminishment of viral replication (lower middle), as well as the tremendous and lethal G-to-A hypermutation (bottom).

certain A3s, a significant frequency of G-to-A mutation in HIV-1 DNA in the presence of Vif is of particular importance for our study. A faint expansion of *vif*-deficient HIV-1 in the humanized mice supports the possibility, indicating that the degradation of certain A3s by Vif is indispensable for HIV-1 replication *in vivo* (Fig. 1D to F). Also, in HIV-1-infected humanized mice, only 3.5% of *vif* genes suffered from a mutation resulting in the termination of translation (Fig. 3B), and the majority of Vif proteins (87.2% of total) maintained the counteracting potential to A3G (Fig. 3C). Nevertheless, we detected a significant G-to-A mutation of HIV-1 DNA harboring the hallmark of A3-mediated mutagenesis in *vif*-proficient HIV-1-infected mice (Fig. 2 and 4). These findings indicate that HIV-1 G-to-A mutation by intrinsic A3s can be evoked even in the presence of Vif. Along with the productive HIV-1 infection in WT HIV-1-infected mice (Fig. 1D to F and 7, top), we detected some HIV-1 amplicons containing tremendous G-to-A hypermutations, which would not be replication competent (Fig. 4B and D). These results suggest that G-to-A hypermutation by endogenous A3s can be partly attributed to the diminished expansion of *vif*-proficient HIV-1 to some extent (Fig. 7, bottom). Moreover, we also detected a significant level of termination-inducible G-to-A mutations (Fig. 2C). Accumulation of stop codon mutations associated with A3-mediated G-to-A substitution has been predicted and actually detected in clinical specimens (reviewed in reference 1). Our result suggests that a moderate level of A3-mediated G-to-A mutation can be a significant factor for the abrogation of viral expansion *in vivo* (Fig. 7, lower middle), which clearly correlates with the findings for HIV-1-infected patients.

In contrast to the findings in proviral DNA, the frequency of multiple G-to-A mutations per amplicon in viral RNA was significantly lower than that in proviral DNA (Fig. 5B). It would be reasonable to assume that hypermutated proviruses were unable to be expressed due to functional defects in their long terminal repeat sequences and/or regulatory genes, resulting in the expression of viral RNA which did not possess a high level of mutations. Moreover, the majority of A3-associated G-to-A mutations detected in viral RNA (74/75) were synonymous (Fig. 5C). These results strongly suggest that A3-mediated mutation under physiological conditions contributes to the abolishment of the replication of *vif*-proficient HIV-1 rather than viral diversity. In addition to the enzymatic ability to elicit G-to-A mutation in proviral DNA, it has been reported previously that A3F and A3G have the potential to impair the plus-strand viral DNA transfer, the formation of proviral DNA, and/or its integration (28, 32). Therefore, the chemical compound(s) that counteracts the function of Vif to degrade certain A3 proteins can be one of the suitable candidates for novel anti-HIV-1 drugs.

The frequency of hypermutated sequences in the samples of infected patients has been estimated to range from approximately 7 to 20% with a large variation (9, 11, 17, 20, 23, 26, 36, 39, 53–55, 57). However, it has been suggested that the G-to-A hypermutated HIV-1 amplicons are difficult to amplify efficiently because of the hypermutation in the primer-binding sequences. In fact, a previous paper (1) has suggested the possibility that extremely hypermutated sequences would fail to replicate and amplify by PCR, which points out that the approximate calculations almost certainly underestimate the total proportion of the sequences mutated by A3s (1). Therefore, although we detected amplicons possessing abundant G-to-A mutations (Fig. 4 and Table 2), it may be difficult to estimate the true frequency of A3-associated G-to-A hypermutants in the total population.

To investigate the variation in an HIV-1 genomic sequence, we used the conventional PCR method. On the other hand, the single-genome amplification (SGA) method is one of the more refined methods to detect low-frequency mutations such as anti-HIV-1 drug-resistant clones and the diversification of the HIV-1 *env* gene and, therefore, has been recently utilized for the sequencing of HIV-1 genomes in patients (8, 37, 42, 48, 57). In this way, only one clone is needed to be amplified by one PCR, which guarantees that amplified sequences come from a single source. Therefore, this technique is a particularly

effective method if the frequency of target sequence in the pool is quite low. However, in this study, we detected relatively higher levels of HIV-1 proviral DNA (Fig. 1E) and viral RNA (Fig. 1D) in WT HIV-1-infected humanized mice than those typically found in patients, providing us with an ample amount of distinct starting material. Moreover, the quantitative data indicate that 301 ± 72 copies of proviral DNA samples or 275 ± 104 copies of viral RNA samples were used per sequencing PCR, respectively. These results imply that conventional PCR is a practical means for evaluating a large population of G-to-A hypermutated amplicons. Albeit that low-frequency mutations may have been excluded in favor of more abundantly occurring mutated amplicons, the sequencing diversity of the amplicons analyzed displayed unique profiles. Indeed, a previous study of the diversity of HIV-1 *env* sequence in a humanized mouse model (14), which used the SGA method for sequencing analysis, detected more diversified HIV-1 RNA sequences than did our study (Fig. 6B). Taken together, the exclusion of low-minority variants might have led to an underestimate in the overall population of mutated amplicons in this study. However, the copy number of proviral DNA per sequencing PCR was comparable to that of viral RNA, which still supports the importance of the idea that proviral DNA sequences were more predominantly diversified than were viral RNA sequences (Fig. 6).

It has been assumed that the HIV-1 quasispecies harboring resistance to conventional anti-HIV-1 drugs can emerge as a result of sublethal A3-mediated G-to-A mutation (20, 33, 40), though this concept is still controversial (18). In proviral DNA, we detected some nonsynonymous G-to-A mutations, which can provide resistance to HIV-1 RT inhibitors (see Fig. S1 in the supplemental material). However, the frequency of drug resistance-associated G-to-A mutation was not remarkable (Fig. 2C). Similarly, after analyzing the mutation frequency in viral RNA, we did not detect A3-associated drug resistance-inducible substitutions (Fig. 5D). These results suggest that endogenous A3-mediated mutagenesis is marginally associated with the acquisition of drug resistance for HIV-1.

It has been proposed that A3-mediated mutagenesis has influenced viral divergence and evolution (18). However, we did not detect a significant increase in A3-associated nonsynonymous mutations that can lead to the emergence of quasispecies (Fig. 2C). In addition, the A3-associated G-to-A mutation in viral RNA was predominantly synonymous substitution (Fig. 5D). In this study, we particularly focused on the influence of A3-mediated mutagenesis on HIV-1 expansion in individual HIV-1-infected mice for 15 weeks and showed strong evidence for the association of A3-mediated mutagenesis with the suppression of viral replication (Fig. 2C and 4C). On the other hand, the human environment allows widespread human-to-human virus transfer for decades. Therefore, our findings would not rule out the possibility that A3-mediated mutagenesis has contributed to viral diversity throughout evolutionary history (Fig. 7, upper middle), as proposed previously (18).

Our humanized mouse model is a useful tool to elucidate the aspects of the relevance between multiple A3 family proteins and HIV-1 hypermutation *in vivo*. As a result, we have herein shown that the editing activity of A3s did not have a profound impact on the emergence of drug-resistant quasispecies or viral diversity but instead led to detrimental termination mutations in HIV-1 provirus, thereby suppressing any additional virus threat. Future investigations using this model will provide us with further understanding of the significance of the mutagenesis caused by intrinsic factors against HIV-1 *in vivo*. Moreover, this model will be one of the adequate candidates to evaluate the capacity of novel anti-HIV-1 drugs that target Vif.

ACKNOWLEDGMENTS

We thank Hiroshi Matsuo (University of Minnesota) and Klaus Strebel (National Institute of Allergy and Infectious Diseases, National Institutes of Health) for critical suggestions about this study and Peter Gee (Institute for Virus Research, Kyoto University) for his generous help in this study. We also express our appreciation for Kotubu Misawa's dedicated support.

This work was supported in part by grants-in-aid from the following: the Ministry of Education, Culture, Sports, Sciences, and Technology, Japan, and the Ministry of Health, Labor and Welfare, Japan (to A.T.-K. and Y.K.); the Sankyo Foundation of Life Science (to A.T.-K.); and the Japan Society for the Promotion of Science for Young Scientists (to K.S.).

REFERENCES

1. **Albin, J. S., and R. S. Harris.** 2010. Interactions of host APOBEC3 restriction factors with HIV-1 *in vivo*: implications for therapeutics. Expert Rev. Mol. Med. **12**:e4.
2. **Bishop, K. N., R. K. Holmes, A. M. Sheehy, N. O. Davidson, S. J. Cho, and M. H. Malim.** 2004. Cytidine deamination of retroviral DNA by diverse APOBEC proteins. Curr. Biol. **14**:1392–1396.
3. **Chelico, L., P. Pham, and M. F. Goodman.** 2009. Mechanisms of APOBEC3G-catalyzed processive deamination of deoxycytidine on single-stranded DNA. Nat. Struct. Mol. Biol. **16**:454–455.
4. **Chiu, Y. L., and W. C. Greene.** 2008. The APOBEC3 cytidine deaminases: an innate defensive network opposing exogenous retroviruses and endogenous retroelements. Annu. Rev. Immunol. **26**:317–353.
5. **Cullen, B. R.** 2006. Role and mechanism of action of the APOBEC3 family of antiretroviral resistance factors. J. Virol. **80**:1067–1076.
6. **Dang, Y., X. Wang, W. J. Esselman, and Y. H. Zheng.** 2006. Identification of APOBEC3DE as another antiretroviral factor from the human APOBEC family. J. Virol. **80**:10522–10533.
7. **Doehle, B. P., A. Schafer, and B. R. Cullen.** 2005. Human APOBEC3B is a potent inhibitor of HIV-1 infectivity and is resistant to HIV-1 Vif. Virology **339**:281–288.
8. **Edmonson, P. F., and J. I. Mullins.** 1992. Efficient amplification of HIV half-genomes from tissue DNA. Nucleic Acids Res. **20**:4933.
9. **Fitzgibbon, J. E., S. Mazar, and D. T. Dubin.** 1993. A new type of G→A hypermutation affecting human immunodeficiency virus. AIDS Res. Hum. Retroviruses **9**:833–838.
10. **Freed, E. O., and M. A. Martin.** 2001. HIVs and their replication, p. 1971–2041. *In* D. M. Knipe and P. M. Howley (ed.), Fields virology, 4th ed., vol. 2. Lippincott Williams & Wilkins, Philadelphia, PA.
11. **Gandhi, S. K., J. D. Siliciano, J. R. Bailey, R. F. Siliciano, and J. N. Blankson.** 2008. Role of APOBEC3G/F-mediated hypermutation in the control of human immunodeficiency virus type 1 in elite suppressors. J. Virol. **82**:3125–3130.
12. **Harari, A., M. Ooms, L. C. Mulder, and V. Simon.** 2009. Polymorphisms and splice variants influence the antiretroviral activity of human APOBEC3H. J. Virol. **83**:295–303.
13. **Harris, R. S., K. N. Bishop, A. M. Sheehy, H. M. Craig, S. K. Petersen-Mahrt, I. N. Watt, M. S. Neuberger, and M. H. Malim.** 2003. DNA deamination mediates innate immunity to retroviral infection. Cell **113**:803–809.
14. **Ince, W. L., L. Zhang, Q. Jiang, K. Arrildt, L. Su, and R. Swanstrom.** 2010. Evolution of the HIV-1 *env* gene in the Rag2$^{-/-}$ $\gamma_c^{-/-}$ humanized mouse model. J. Virol. **84**:2740–2752.
15. **Ito, M., H. Hiramatsu, K. Kobayashi, K. Suzue, M. Kawahata, K. Hioki, Y. Ueyama, Y. Koyanagi, K. Sugamura, K. Tsuji, T. Heike, and T. Nakahata.** 2002. NOD/SCID/γ_c^{null} mouse: an excellent recipient mouse model for engraftment of human cells. Blood **100**:3175–3182.
16. **Izumi, T., K. Shirakawa, and A. Takaori-Kondo.** 2008. Cytidine deaminases as a weapon against retroviruses and a new target for antiviral therapy. Minirev. Med. Chem. **8**:231–238.
17. **Janini, M., M. Rogers, D. R. Birx, and F. E. McCutchan.** 2001. Human immunodeficiency virus type 1 DNA sequences genetically damaged by hypermutation are often abundant in patient peripheral blood mononuclear cells and may be generated during near-simultaneous infection and activation of CD4$^+$ T cells. J. Virol. **75**:7973–7986.
18. **Jern, P., R. A. Russell, V. K. Pathak, and J. M. Coffin.** 2009. Likely role of